Am J Cancer Res 2023;13(12):5950-5965
www.ajcr.us /ISSN:2156-6976/ajcr0152127

Original Article

Genome-wide analysis of circulating tumor DNA methylation profiles in cerebrospinal fluid: a clinical trial of oncolytic virus for glioblastoma

Lin Dai[1], Zixuan Jing[1], Yi Zhu[1], Kaihan Deng[1], Lixin Ma[2,3]

[1]*Department of Neurosurgery, Binzhou Medical University Hospital, Binzhou 256603, Shandong, P. R. China;*
[2]*Department of Neurosurgery, Beijing Chaoyang Hospital, Capital Medical University, Beijing 100020, P. R. China;*
[3]*Department of Neurosurgery, Sanbo Brain Hospital, Capital Medical University, Beijing 100093, P. R. China*

Received July 10, 2023; Accepted October 11, 2023; Epub December 15, 2023; Published December 30, 2023

Abstract: Glioblastoma (GBM) is a common malignant tumor of the central nervous system with a poor prognosis and a short survival period. A novel tumor oncolytic virus, Ad-TD-nsIL-12, has manifested anti-tumor properties in preclinical studies. However, the genetic changes caused by Ad-TD-nsIL-12 after GBM treatment are unclear. Therefore, we collected cerebrospinal fluid and tumor tissues from patients injected with Ad-TD-nsIL-12 at different time points and analyzed the methylation and expression profiles of cerebrospinal fluid-derived circulating tumor DNA (ctDNA). The differential genes were screened using the least absolute selection and shrinkage operator (LASSO) and Cox regression analyses. The CIBERSORT algorithm was used to assess the abundance of glioma immune cell infiltration in The Cancer Genome Atlas (TCGA) dataset. The role of hub genes in the diagnosis, prognosis, and immune cell correlation was analyzed using R software, SPSS software, and GraphPad Prism. The results showed that after Ad-TD-nsIL-12 injection, 3631 differential methylation regions (DMRs) were up-regulated and 497 DMRs were down-regulated. The methylation levels of these DMRs recovered within 70 to 82 days. Combined with the TCGA dataset, 8 key genes were selected for the construction of diagnostic and prognostic models. There was a significant correlation between core genes and immune cells. The results revealed that the hub genes in CSF could be used as a biomarker for the diagnosis and prognosis of GBM and led us to speculate the effect of the hub gene on the immune mechanism underlying Ad-TD-nsIL-12.

Keywords: Ad-TD-nsIL-12, liquid biopsy, ctDNA, methylation, glioblastoma

Introduction

Glioma is the most common primary intracranial malignancy, accounting for 80% of central nervous system (CNS) malignancies and about 27% of neurological tumors, and is one of the malignancies with the worst prognosis and highest mortality rate in humans [1]. Currently, no satisfactory treatment is available for GBM. The standard of care is maximal surgery, radiation therapy, and temozolomide synchronized chemotherapy, but the five-year survival rate of GBM patients is low [2, 3]. Thus, a new treatment method is an urgent clinical requirement to improve the survival rate of GBM patients and improve the current treatment status of the disease.

Immunotherapy has received increasing attention in the last decades in modern oncology, and many immunotherapeutic approaches have been developed, which include oncolytic viruses (OVs) [4]. These viruses can selectively multiply in tumor cells and have a low impact on normal cells [5]. The mechanism of action of OVs is not limited to direct tumor lysis of cancer cells and has immunomodulatory effects that enhance the anti-tumor response of the immune system [6-9]. According to a previous study, the dramatic response and long-term survival of the oncolytic adenovirus DNX-2401 in the treatment of high-grade gliomas were ascribed to the direct oncolytic effect of the virus and elicited an immune-mediated anti-tumor response [10]. In the present study, we used a novel oncolytic adenovirus, Ad-TD-nsIL-12, which seems promising for cancer treatment in animal models [11]. This oncolytic adenovirus is based on the five-base adenovirus Ad-TD with the deletion of 3 genes, *E1ACR2*,

E1B19K, and *E3gp19K*, but with the retention of the *E3B* gene. Ad-TD-nsIL-12 transferred non-secretory (ns) interleukin 12 (IL-12) into tumor cells and significantly improved the survival in a Syrian hamster model of pancreatic cancer. IL-12 is a strong immunomodulator that exerts anti-tumor effects by activating dendritic cells, macrophages, natural killer (NK) cells, and cytotoxic T lymphocytes (CTLs) [12]. It promotes interferon-gamma (IFN-γ) production by these cells, thereby developing anti-tumor immunity and inhibiting tumor angiogenesis [13, 14]. However, IL-12 causes a systemic inflammatory response, greatly hindering clinical use [15]. Typically, Ad-TD-nsIL-12 inhibits tumor growth and angiogenesis and improves the survival rate of experimental animals without significant toxic side effects, which brings new hope for tumor treatment in the clinic. Nevertheless, the therapeutic efficacy of Ad-TD-nsIL-12 in animal models has been confirmed, but its immune mechanism, treatment period, and injection dose in GBM treatment are unknown, needing further studies and clinical trials to substantiate the current findings.

Although tissue biopsy is the gold standard method for diagnosing and predicting patients with glioma, many studies have recently emphasized the drawbacks of this approach [16, 17]. First, tissue samples are not fully representative of tumor heterogeneity, limiting the accuracy of prediction results [18]. In addition, because tissue biopsy sampling is a highly invasive intervention and extremely difficult because of the poor anatomical location of the tumor; also, it is also difficult to detect early diagnosis, residual conditions, and disease recurrence [19]. Therefore, a minimally invasive method is an urgent requirement to detect cancer early and facilitate patient follow-up. Liquid biopsy (LB) can be a viable method to overcome these drawbacks. Recently, LB has become a hotspot for diagnostic research worldwide. It identifies and monitors tumor biomarkers, such as circulating tumor cells (CTCs), circulating tumor DNA (ctDNA), and exosomes at the molecular level using human blood, cerebrospinal fluid (CSF), urine, saliva, and other body fluids [20]. Compared to pathological tissue biopsy, LB has the advantages of real-time monitoring, reproducibility, and non-invasiveness, enabling early diagnosis of tumors, disease monitoring, individualized treatment, targeted drug use, prognosis assessment, and recurrence monitoring [21, 22]. Therefore, this non-invasive diagnostic method that involves collecting samples from patients' body fluids could be a new alternative to traditional pathological tissue biopsies [23, 24].

ctDNA is a double-stranded DNA fragment released into the circulatory system by apoptosis, necrosis, or direct secretion from tumor cell DNA and is a biomarker carrying genetic information of the tumor genome [25]. On the other hand, DNA methylation is one of the most widely studied epigenetic modifications in humans, and the underlying epigenetic mechanism is the covalent addition of methyl groups provided by S-adenosylmethionine (SAM) to the five-position carbon of the cytosine ring to form 5-methylcytosine. Abnormal DNA methylation is one of the hallmarks of many cancers, with methylation changes occurring early in the life of the carcinogen [26]. Therefore, the present study aimed to investigate the therapeutic process, immune mechanism, treatment period, and injection dose of Ad-TD-nsIL-12 by analyzing CSF ctDNA methylation of GBM patients.

Materials and methods

Samples

GBM CSF and tissue samples were obtained from one patient enrolled in the clinical trial at the Department of Neurosurgery, Sanbo Brain Hospital, Capital Medical University (Beijing, China). All samples were diagnosed pathologically, and tumor tissues were stored at -80°C after rapid freezing in liquid nitrogen. All patients signed an informed consent form for the protocol approved by the local institutional review board (SBNK-YJ-2020-001-0).

Sample information

The average survival time for GBM is 15 months, while the survival time for patients with recurrent GBM is only 6 months [27]. However, in one of our clinical trials, a GBM patient who relapsed after treatment with the oncolytic virus Ad-TD-nsIL-12 survived for approximately 12 months with significantly prolonged progression-free survival. In addition, magnetic resonance imaging (MRI) displayed a reduction in the abnormal tumor signals after injection of Ad-TD-nsIL-12. Therefore, we col-

lected CSF and tissue samples from this patient at different treatment time points for methylation and transcription profiling (Supplementary Figure 1B). In September 2019, the patient was diagnosed with diffuse midline glioma, H3K27M mutant type, World Health Organization (WHO) grade IV. Then, the patient was treated with tumor resection, concurrent radiotherapy, and chemotherapy (temozolomide 200 cGy × 27 f.). In February 2021, the patient's cranial MRI exhibited abnormal signals in the left thalamic floor area, right medial thalamus, and left brain side, implying tumor recurrence.

The MRI information of this patient is shown in Supplementary Figure 1A. The patient's time to collect CSF and tissue is shown in Supplementary Table 1. In addition, we collected one normal tissue sample from internal compression tissue from a patient undergoing brain decompression.

Extraction and methylation sequencing of ctDNA

The DNeasy kit (Qiagen Inc., Germany) was used according to the manufacturer's instructions to extract ctDNA from G1-G5 CSF samples and sequence them for methylation. We used a portion of CSF samples from G1 and a portion of normal CSF as input samples for this sequencing, named G1. Input and N.Input, thus reducing the false positive rate of sequencing. The other samples were named G1.IP, G2.IP, G3.IP, G4.IP, G5.IP, and N.IP, and the subsequent studies were correspondingly referred to as G1, G2, G3, G4, G5, and N.

High-throughput sequencing was provided by Cloud-Seq Biotech (Shanghai, China). Phenol-chloroform was used to isolate genomic DNA, followed by precipitation with ethanol and ultrasonication by Biof corruptor (diagenetic carols) to fragments of 100-500 bl. NEBNext® Ultra™ DNA Library Prep Kit (NEB) was used for ultrasonic DNA repair at the end, and a tail was connected to the adapter. Then, monoclonal antibodies were used to resist 5-methylcytosine via a standard manufacturer agreement (Active Motif) MeDIP. The Quant-iT PicoGreen dsDNA Kits (Life Technologies) were used following the manufacturer's recommendations for a quantitative MeDIP DNA library, followed by high-throughput sequencing of 150 base pairs at the C-terminal on an Illumina HiSeq machine.

The Illumina NovaSeq 6000 sequencing machine generates raw data after sequencing, image analysis, tone, and quality filtration. First, Q30 was used for quality control. Then, adapter pruning and Cutadapt (v1.9.3) software were used to remove the low-quality reads and generate high-quality clean reads. Next, bowtie2 software (v2.2.4) was used, and the default parameters of the clean reads were set using the human genome (HG19) as the reference. Peaks were called by MACS software (V2.0). The diffReps software (v1.55.4) was used to identify the differences between methylation areas. Finally, the latest UCSC RefSeq database was used to annotate methylation AR and EA and connect peak information and gene annotations.

Extraction of tumor mRNA and sequencing of gene expression profile

Tumor tissue samples were collected from this patient before injecting Ad-TD-nsIL-12. The rRNAs in the total RNA were isolated using Ribo-Zero rRNA Removal Kits (Illumina, USA) according to the manufacturer's instructions. For high-throughput sequencing of RNA by Cloud-Seq Biotech (Shanghai, China), NEBNext rRNA exhausted kits (New England Biolabs, Inc., MA, USA) were used to isolate the RNA from total RNA. Next, Directional RNA libraries were built using the NEBNext® Ultra™ II library preparation kit (New England Biolabs, Inc.), according to the manufacturer's specifications. Subsequently, the 2100 BioAnalyzer system (Agilent Technologies, Inc., USA) was used to control the library quality by Q30 and quantitation, followed by sequencing on the Illumina NovaSeq 6000 instrument. Then, three adapter clippings and low-quality reads were removed using Cutadapt software (V1.9.3), and high-quality clean reads were aligned against the human reference genome (HG19) using Hisat2 software (V2.0.4). Finally, HTSeq (v0.9.1) was used to obtain the original count, using the normalized edgeR, applying the *p*-value and a fold-change to identify the differentially expressed mRNA.

Selection and analysis of the cancer genome atlas (TCGA) database samples

Gene expression profiles and clinical data for 698 glioma and 5 normal samples were downloaded from the TCGA (https://www.cancer.

gov/). Some samples with incomplete clinical information were removed from these 703 samples, and finally, 665 were included in the LASSO regression analysis and multifactorial Cox regression analysis.

Statistical analysis and image construction

The present study used R software (v.3.6.3), SPSS software (v.24, IBM), and GraphPad Prism (v.8.0.2) for statistical analysis and graph plotting. The samples in the TCGA dataset were analyzed for differences using the "limma" R packages and considered statistically significant at $P < 0.05$ [28]. Kaplan-Meier (KM) curves described the survival distribution. Univariate analysis was used to identify the survival-associated hub genes, and the "survival" and "survminer" R packages were applied for our analysis (https://CRAN.R-project.org/package=survival). Prognostic models were analyzed and screened for prognostic gene markers using LASSO regression analysis. The prognostic genetic markers were calculated as risk scores using the "survival" R package and divided into high- and low-risk groups according to the median of the risk scores. To investigate the correlation between multigene association and immune cells, we applied multi-correlation analysis with SPSS software and considered it statistically significant when r (Pearson's correlation coefficient) > 0.3 and $P < 0.05$. In addition, the diagnostic receiver operational characteristic (ROC) curve of multigene association was analyzed using SPSS software. The predictors of the genes and their ROCs were estimated using binary logistic regression analysis.

Results

Overall sample characteristics

To determine whether Ad-TD-nsIL-12 treatment altered the distribution and size of the GBM CSF ctDNA methylation region, we visualized the sequencing results of the samples using IGV software (version 2.11.8). The results showed differences in the methylation peaks of normal samples, samples not injected with Ad-TD-nsIL-12, and samples injected with Ad-TD-nsIL-12 (Supplementary Figure 2A, 2B). The normal CSF samples had high methylation levels, while tumor CSF samples (including those injected with Ad-TD-nsIL-12) exhibited hypomethylation levels in some regions. Supplementary Figure 3A shows that the methylation regions of CSF ctDNA on chromosomes did not show differences between the groups of samples. Nevertheless, the proportion of CSF ctDNA methylated regions distributed on genomic elements (promoter 4.26-7.68%, upstream 14.38-17.56%, intron 29.16-32.76%, exon 1.51-3.42%, and intergenic 41.02-49.85%), methylation regions (380-500 bp), and the proportion of normalized tag-fold enrichment distribution (most of the fold enrichment were less than 10) were similar in all groups of samples (Supplementary Figure 3B-D). The normalized tag-fold enrichment is a parameter obtained from IP samples vs. input samples and can be interpreted as the peak of the methylation region.

ctDNA methylation level in CSF changes after Ad-TD-nsIL-12 injection

To analyze the changes in the methylation regions before and after Ad-TD-nsIL-12 treatment, we analyzed the differences between two samples: G2 vs. G1, G3 vs. G2, G4 vs. G3, G5 vs. G4. The levels of some methylation regions were altered (up- or downregulated) after Ad-TD-nsIL-12 injection and fully or partially restored to the original methylation levels after 70-82 days (**Figure 1C** and **1D**). Consequently, the methylation levels of 3631 genes were upregulated after two injections of Ad-TD-nsIL-12 but were recovered (**Figure 1A**) after 70-82 days. On the contrary, the methylation levels of 497 genes were downregulated after two injections of Ad-TD-nsIL-12 and upregulated 70-82 days after the injection (**Figure 1B**).

Characterization of gene expression in tumor tissues and screening of hub genes

Differential genes under specific conditions (including differentially methylated region-associated genes and differentially expressed genes) were used to identify the hub genes after Ad-TD-nsIL-12 treatment. The results showed altered gene expression levels in tissue samples injected with Ad-TD-nsIL-12 (**Figure 2C**), although T3 was collected 70 days after the first injection of oncolytic adenovirus. The partially upregulated genes after the injection of Ad-TD-nsIL-12 recovered after a specific period (**Figure 2A** and **2B**). Next, we intersected the differentially expressed genes in tumor tissues (T3 vs. T1; 91 genes) with genes associated with CSF ctDNA DMRs (G3 vs. G1; 9113 genes)

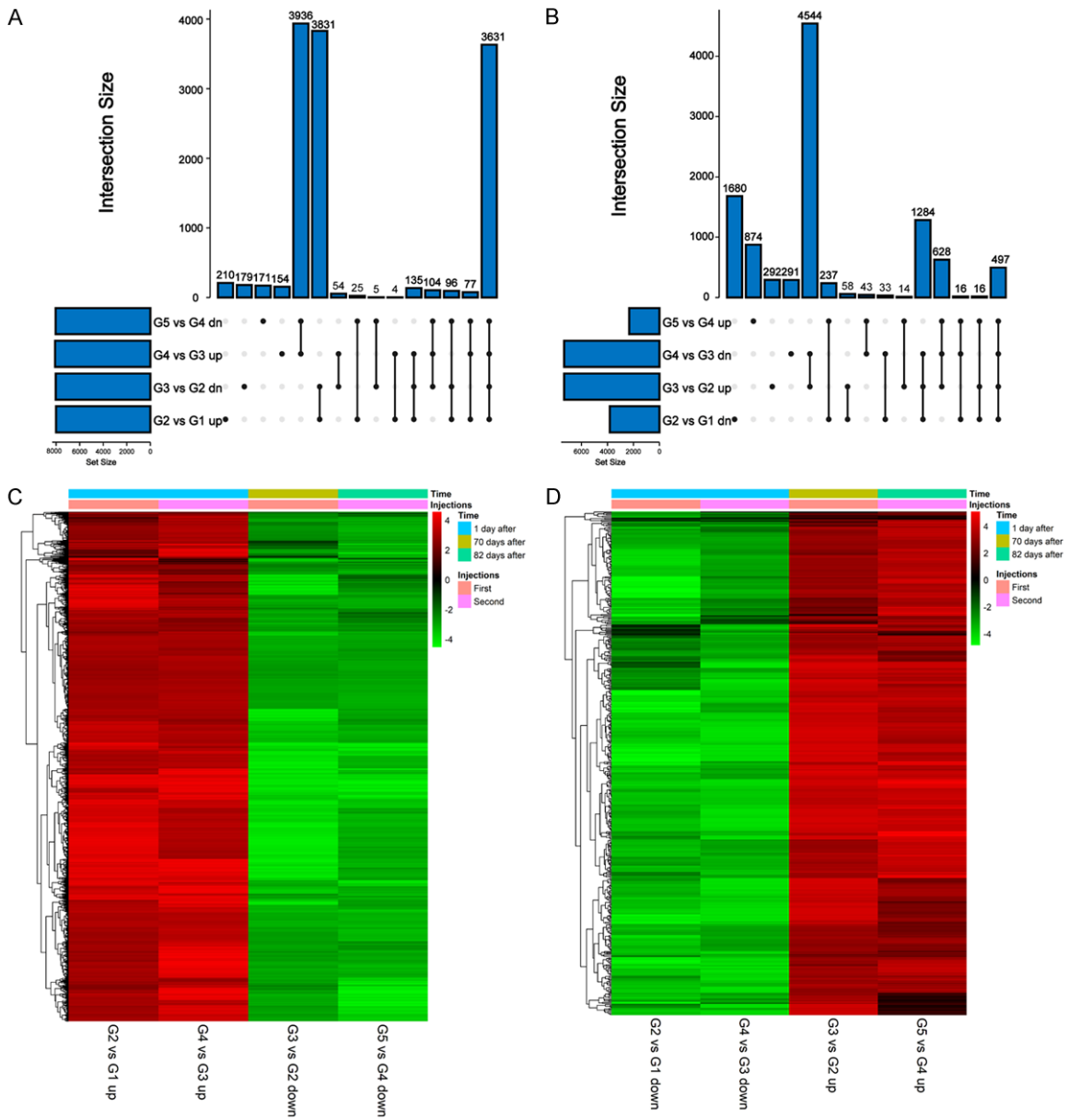

Figure 1. Changes in CSF ctDNA methylation levels after Ad-TD-nsIL-12 injection. A. Several genes were upregulated in DMRs after two injections of Ad-TD-nsIL-12. B. Several genes were downregulated in DMRs after two injections of Ad-TD-nsIL-12. C, D. Heatmap of fold-enrichment after logarithmic comparison of the two groups. Red indicates the upregulation of fold enrichment, and green indicates the downregulation of fold enrichment.

and those altered after injection (3774 genes; **Figure 2D**). Ultimately, 26 genes were selected (*CD5*, *SCML4*, *CD2*, *EBI3*, *POU2AF1*, *LY86*, *PCP4*, *GZMB*, *DUSP27*, *CRTAM*, *CCR2*, *CACNA1F*, *LCN2*, *MUC5B*, *B3GNT3*, *EPPK1*, *CCNJL*, *KRT8*, KRT80, *ELF3*, *KLF5*, *ESRP2*, *ANKRD34B*, *IER3*, *NGF*, and *PLAU*) from the intersection of differential genes of tissue samples and pairing CSF ctDNA methylation samples, and 4 genes (*CALN1*, *GRHL2*, *MUC4*, and *C1QL3*) from the intersection of the 3 groups (tissue group, CSF group and changing group after injection) were selected for inclusion in the subsequent analysis. Subsequently, 91 differential genes with P < 0.1 were selected from T3 s. T1 was included in the analysis.

Gene Ontology (GO) and Kyoto Encyclopedia of Genes and Genomes (KEGG) pathway analysis of genes corresponding to promoter DMRs of CSF ctDNA

To detect the function of genes associated with CSF ctDNA DMRs, those with promoter DMRs

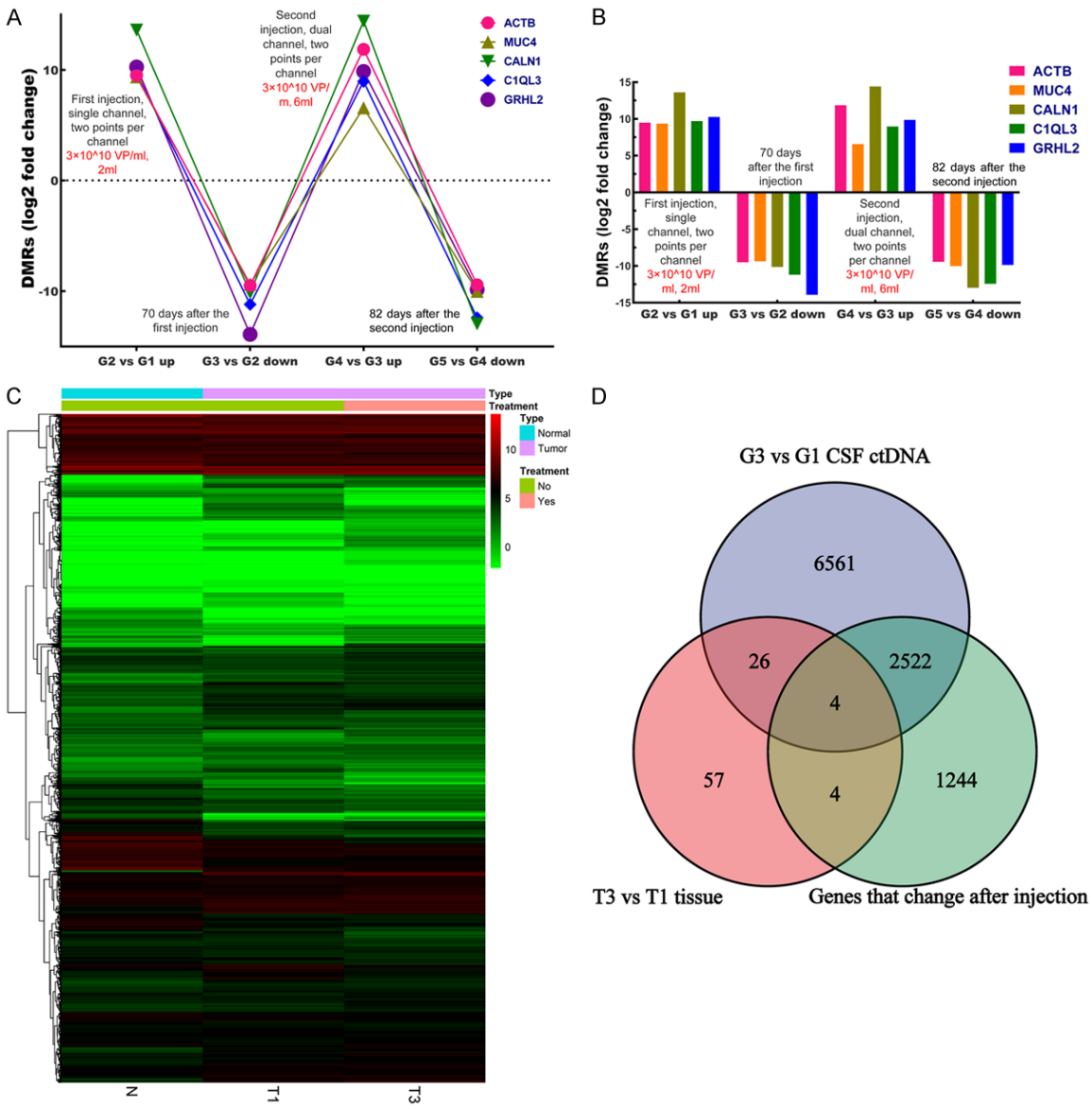

Figure 2. Characterization of gene expression in tumor tissues and screening of hub genes. A, B. A subgroup of DMR-related genes with changes in log2 fold-change after Ad-TD-nsIL-12 injection. C. Heatmap of gene expression levels in tumor tissue samples and normal tissue gene expression levels. D. Venn diagram of the intersection among differential genes of tissue samples (T3 *vs*. T1), pairing CSF ctDNA methylation samples (G3 *vs*. G1), and 3774 DMR-related genes (including 3631 up- and 497 downregulated genes).

were subjected to GO analysis, including biological processes (BP), molecular functions (MF), and cellular components (CC) (**Figure 3A-D**, Supplementary Figure 4A-D). The top eight entries showed the enrichment score. The major BPs involved in genes associated with the first injection of Ad-TD-nsIL-12 DMRs were protein modification by small protein removal via deubiquitination and mitotic G1/S transition checkpoint. On the other hand, the BPs involved in the genes associated with the methylation regions induced by the second injection of Ad-TD-nsIL-12 negatively regulated the cellular protein catabolic process, proteolysis involved in cellular protein catabolic process, and snRNA 3'-end processing.

In addition, analysis of the top eight KEGG pathways for enrichment scores of DMRs upregulated after injection revealed that the pathways involved in genes associated with CSF ctDNA DMRs included pathways associated with sys-

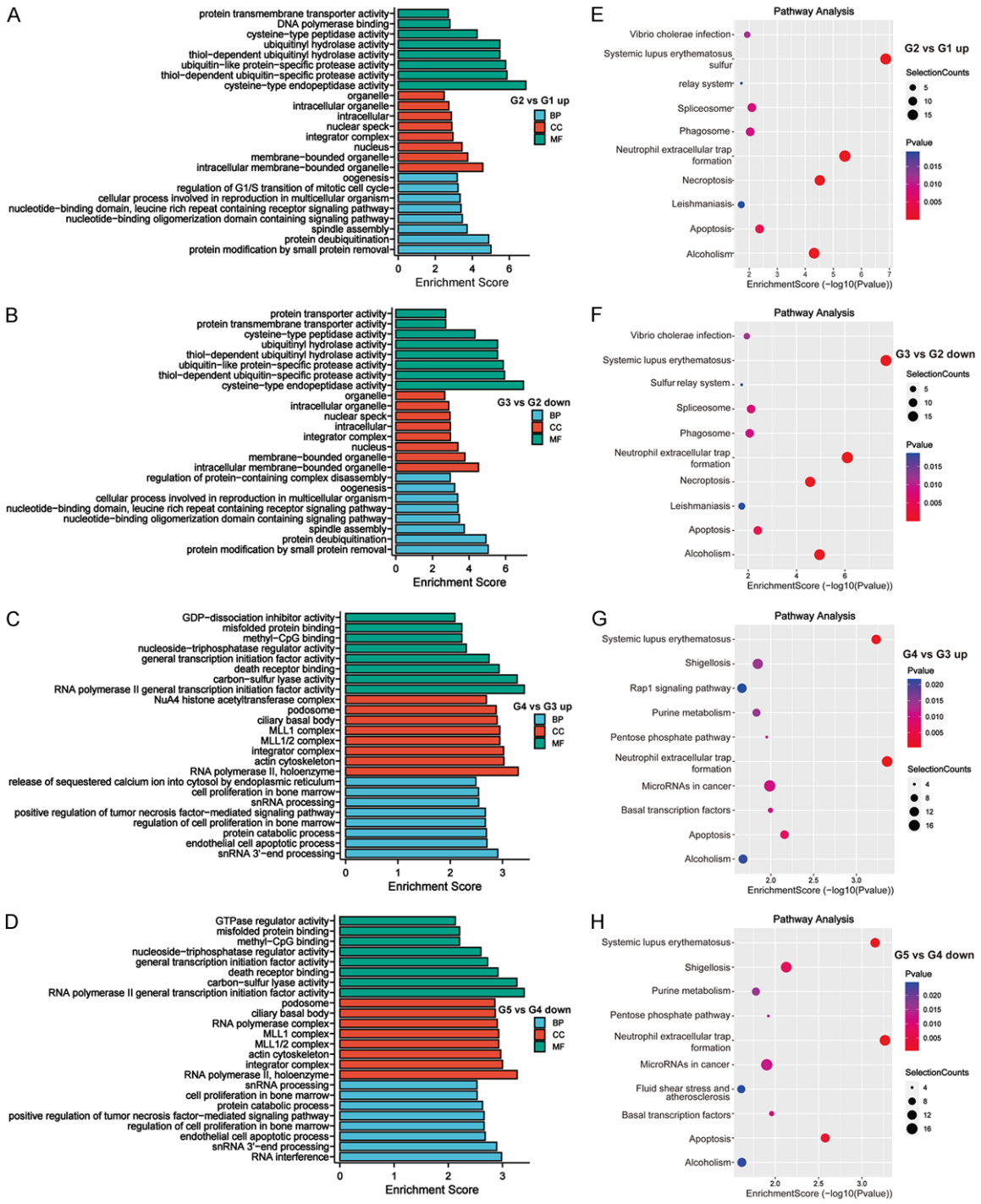

Figure 3. GO and KEGG analysis of genes associated with promoter DMRs of CSF ctDNA. A-D. CSF ctDNA promoter DMRs are associated with gene enrichment scores for the top eight terms of GO analysis. E-H. CSF ctDNA promoter DMRs-associated gene enrichment fraction of the top eight terms of the KEGG pathway.

temic lupus erythematosus, neutrophil extracellular trap formation, alcoholism, and apoptosis (**Figure 3E-H**, Supplementary Figure 4E-H). These four pathways were present in all four sets of comparison samples, G2 vs. G1 up, G3 vs. G2 down, G4 vs. G3 up, and G5 vs. G4 up, and they shared 6 genes related to DMRs: *ACTB*, *PARP2*, *RIPK1*, *H2AFB1*, *H2AFB2*, and *H2AFB3*. However, *H2AFB1*, *H2AFB2*, and *H2AFB3* did not appear in the gene expression

profile, and hence, ACTB, PARP2, and RIPK1 were included in the follow-up analysis.

Validation of the role of the 33 genes screened from public databases

To validate the significance of these 33 genes (including genes screened in the CSF ctDNA and KEGG pathways), we analyzed them in conjunction with public databases. The gene expression profiles of 698 glioma samples and 5 paraneoplastic samples were collected from the TCGA database, excluding those with incomplete clinical data, and finally including 665 samples in the follow-up part of the study. According to the univariate Cox regression model, 24 hub genes (Supplementary Table 2) were significantly associated with OS. Subsequently, 8 hub genes were screened by LASSO regression analysis (**Figure 4A**) and multifactorial Cox analysis; *CALN1*, *GZMB*, *DUSP27*, *KRT80*, *CD5*, *CCNJL*, *LCN2*, and *ACTB* were identified to construct the prognostic and diagnostic models (**Figure 4B**). The comparison of the expression profiles of these 8 hub genes with the expression profiles in the TCGA dataset showed differences in the expression of *ACTB*, *CALN1*, *CCNJL*, and *DUSP27* ($P < 0.05$; **Figure 4C-J**). After dividing the hub genes into high- and low-expression groups, the levels of *CALN1* and *DUSP27* genes were positively correlated with OS ($P < 0.001$), while the expression levels of *ACTB*, *CCNJL*, *CD5*, *GZMB*, KRT80, and *LCN2* genes were negatively correlated with OS ($P < 0.001$; Supplementary Figure 5).

Distribution of immune infiltrates in gliomas and analysis of immune cell correlations in 8 hub genes

Ad-TD-nsIL-12, one of the methods of immunotherapy, can achieve anti-tumor effects by altering the number of immune cells in the tumor microenvironment. Therefore, 8 hub genes were combined with glioma immune cell infiltration abundance to analyze the correlation between hub genes and immune cells.

Based on glioma data from TCGA, we assessed the abundance of 22 immune cell species in gliomas using CIBERSORT, as described previously [29, 30]. Five normal samples in TCGA were not included in the analysis related to immune infiltration. Supplementary Table 3 and Supplementary Figure 6 show that 14 immune cells were significantly associated with OS ($P < 0.05$): macrophages M0, macrophages M1, macrophages M2, monocytes, neutrophil and NK cell activation, mast cell activation, mast cell quiescence, eosinophils, T cell CD4 memory, T cell CD4 naïve, T cell CD8, T cell γδ, and regulatory T cells (Tregs). The results of the analysis revealed a statistical correlation between the hub genes and some immune cells ($|r| > 0.3$, $P < 0.05$) (**Figure 5A**). Interestingly, these immune cells with significant correlations with hub genes ($|r| > 0.3$, $P < 0.05$) were deemed OS-associated immune cells. Therefore, hub genes associated with immune cells ($|r| > 0.3$, $P < 0.05$) were used for multiple correlation analysis to investigate the linear association of multiple variables with immune cells. The results of multi-correlation analysis displayed that the hub genes are associated with monocytes ($r = 0.685$), macrophages M0 ($r = 0.658$), macrophages M1 ($r = 0.468$), T cells CD4 memory activated ($r = 0.525$), and T cells CD8 ($r = 0.362$), but no correlation was established with macrophages M2 ($r = 0.21$) (**Figure 5B**, **5C**, Supplementary Figure 7). In addition, no multiple correlation analysis was conducted to elucidate the association of hub genes with neutrophils and activated NK cells, as only one hub gene was significantly associated with both immune cells ($|r| > 0.3$, $P < 0.05$).

Prognostic models were constructed based on 8 hub genes

Based on the expression of hub genes in the TCGA dataset, risk scores were calculated for 665 glioma samples and high- and low-risk groups were distinguished according to the median risk score; significant differences were detected between the high- and low-risk groups ($P < 0.001$) (**Figure 6A**). Subsequently, to assess the predictive ability of this prognostic model, the area under the ROC curve (AUC) corresponding to 1, 3, and 5 years was calculated as 0.860, 0.914, and 0.839, respectively (**Figure 6B**). Patients had a poor prognosis as the survival time and risk score increased (**Figure 6C**, **6D**). In addition, the expressions of *GZMB*, *KRT80*, *CD5*, *CCNJL*, and *ACTB* were positively correlated with the risk score of patients, whereas the expressions of *LCN2*, *CALN1*, and *DUSP27* were negatively correlated with the risk score of patients (**Figure 6E**).

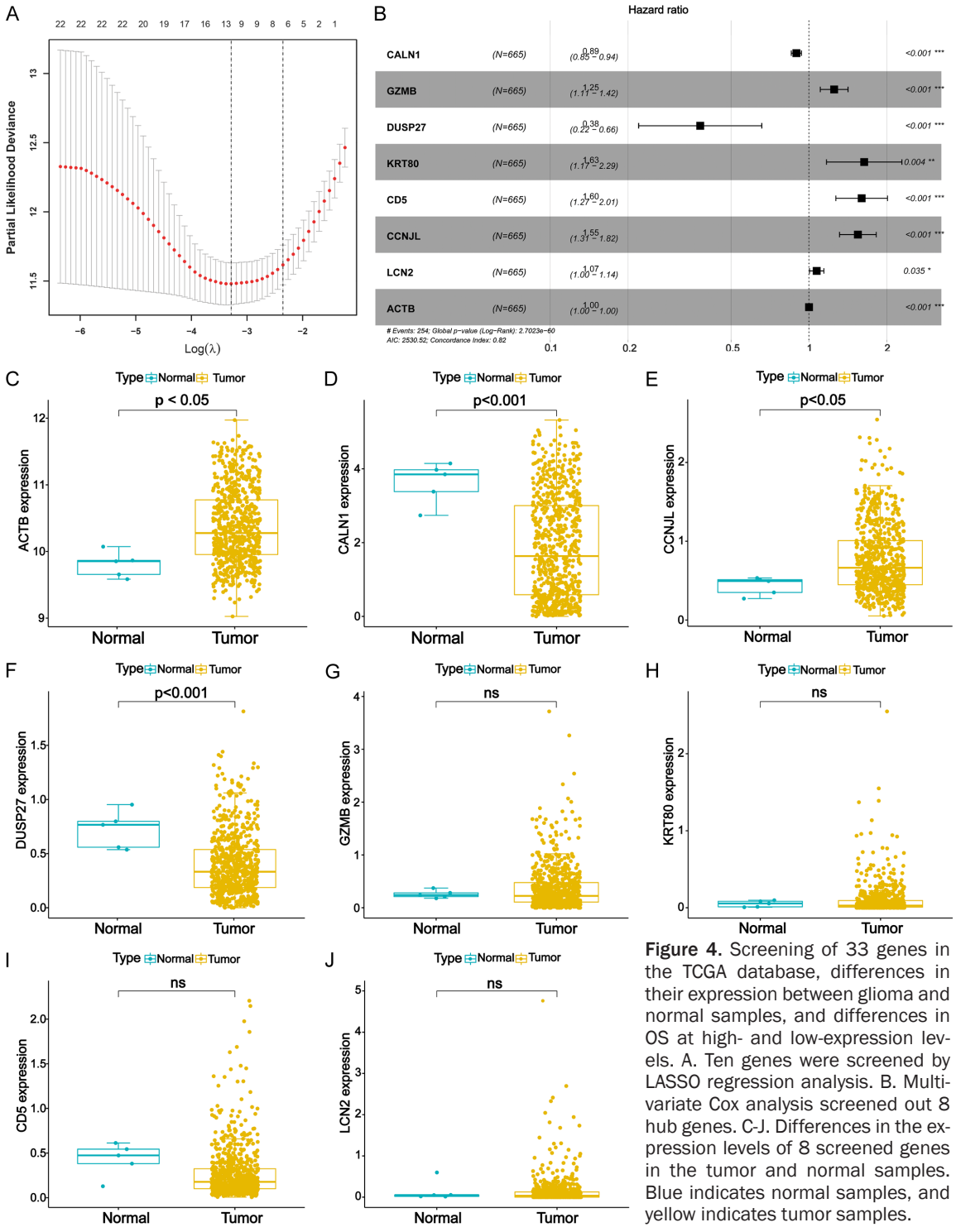

Figure 4. Screening of 33 genes in the TCGA database, differences in their expression between glioma and normal samples, and differences in OS at high- and low-expression levels. A. Ten genes were screened by LASSO regression analysis. B. Multivariate Cox analysis screened out 8 hub genes. C-J. Differences in the expression levels of 8 screened genes in the tumor and normal samples. Blue indicates normal samples, and yellow indicates tumor samples.

Diagnostic models were constructed based on 8 hub genes

Binary logistic regression analysis was performed based on the expression of 8 hub genes in 698 glioma samples and 5 normal samples from the TCGA dataset. The combined diagnostic ROC of these genes was analyzed by calculating the diagnostic predictors of the 8 genes. The results depicted that the AUC values of *ACTB* (0.828), *CALN1* (0.853), *CCNJL* (0.761), *CD5* (0.752), and *DUSP27* (0.848) were high,

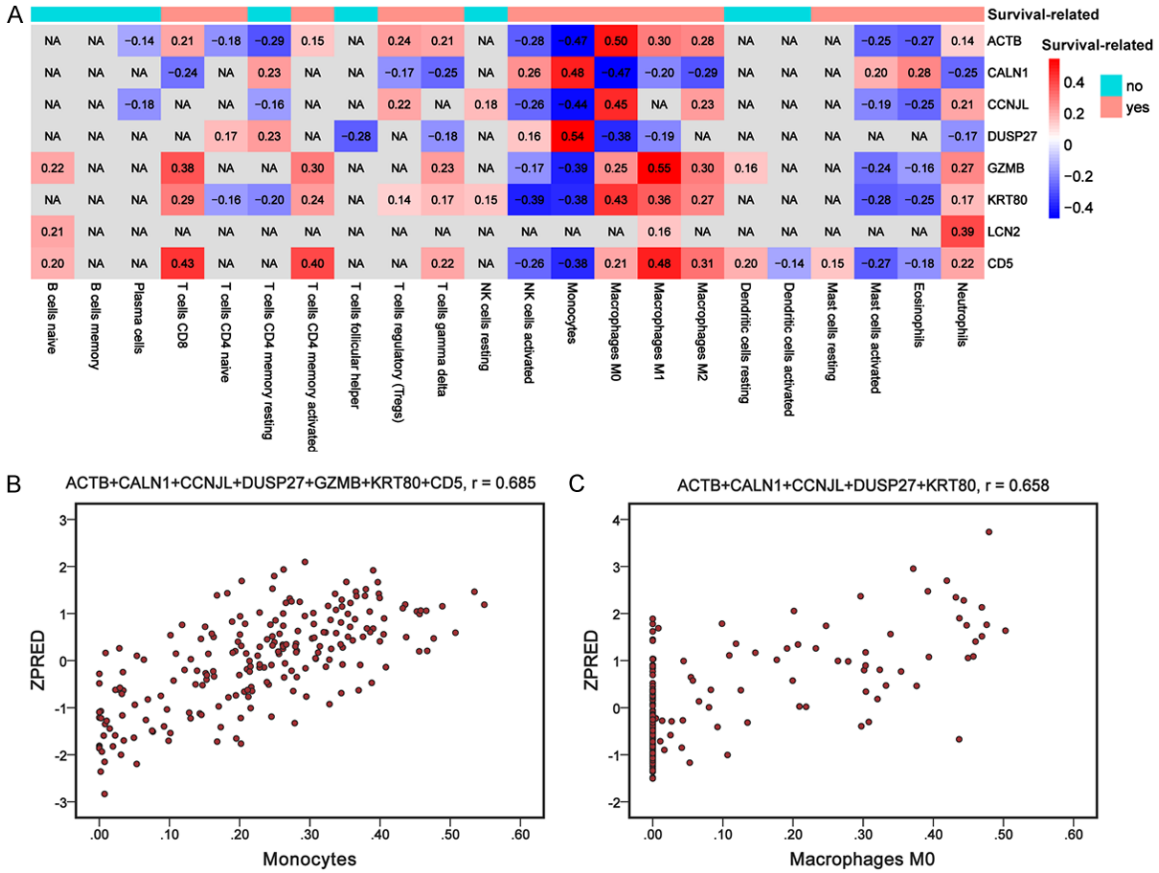

Figure 5. Correlation analysis of 22 immune cells with OS and hub genes. A. Heatmap of hub gene correlation with immune cells. Red indicates a positive correlation, blue indicates a negative correlation, and NA indicates P > 0.05. B, C. Multi-correlation analysis of hub genes associated with monocytes and macrophage M0 ("r" denotes multi-correlation coefficient).

while the AUC values of *GZMB* (0.467), *KRT80* (0.478), and *LCN2* (0.432) were low (Supplementary Figure 8A). The combined diagnostic ROC analysis of *ACTB*, *CALN1*, and *DUSP27* had a higher AUC (AUC = 0.919) than that of univariate diagnostic ROC (Supplementary Figure 8B).

Discussion

DNA methylation is one of the first epigenetic regulatory patterns that have promising applications in classifying and diagnosing GBM [31-34]. This phenomenon is attributed to abnormal hypermethylation of cytosine-phosphate-guanine (CpG) islands in tumor suppressor genes that may lead to transcriptional silencing and cancer development [35]. The abnormal methylation pattern has been detected in many studies as an early event in cancer development and as a reversible change [36, 37]. Thus, we attempted to identify the key targets of Ad-TD-nsIL-12 for tumor treatment by methylation profiles of ctDNA extracted from CSF. On the other hand, ctDNA can be collected from the plasma of tumor patients for testing [38]. This approach does not apply to CNS tumors because ctDNA in CNS tumors has difficulty entering the circulatory system due to the blood-brain barrier. CNS tumors are often in contact with CSF, such that ctDNA extraction from CSF may be better than that from plasma for real-time monitoring of disease progression and treatment response [39, 40]. The epigenetic features inherent to brain tumors in situ have a high probability of preservation in CSF ctDNA; hence, detecting CSF ctDNA methylation levels may be a sensitive and accurate method for monitoring response to brain tumor therapy progression, survival, and recurrence [41]. Currently, the mechanism of Ad-TD-nsIL-12 in clinical treatment is unclear. Based on our

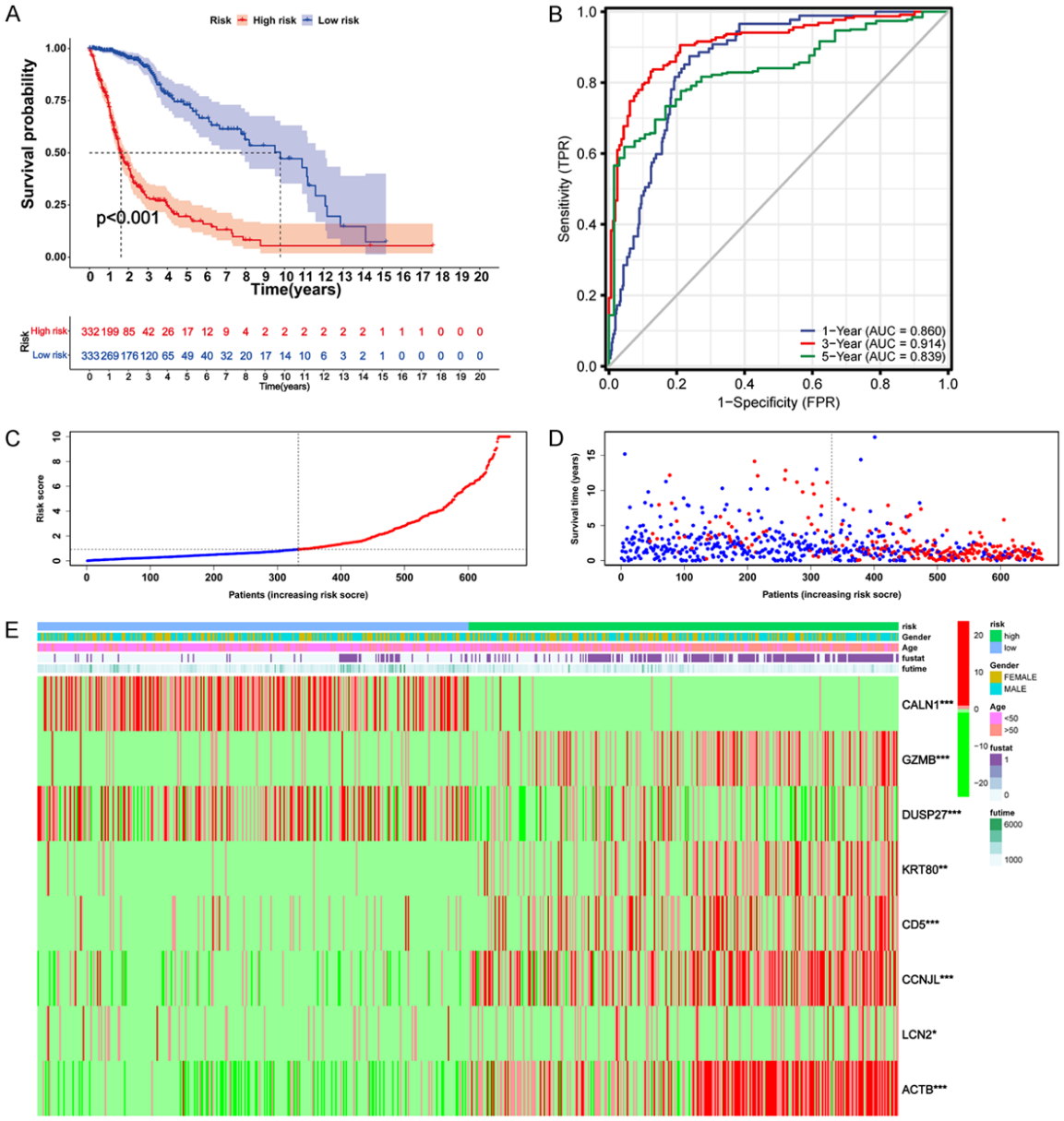

Figure 6. Risk prediction models on 8 genes. A. KM survival curves for high- and low-risk groups with OS. Red indicates the high-risk group, and blue indicates the low-risk group. The table below indicates the sample size of high- and low-risk groups for different survival times. B. Time-dependent ROC at 1, 3, and 5 years based on 8 hub gene signatures. C. Risk curves are based on 8 hub gene prognostic models. Red indicates the high-risk group, blue indicates the low-risk group, and the dashed line indicates the median value. D. Overview of survival based on 8 hub gene prognostic models. Red indicates dead; blue indicates alive. E. Heatmap of the relationship between the expression levels of 8 genes and multiple factors. Red indicates high expression, and green indicates low expression.

observations of the response of Ad-TD-nsIL-12 treatment in the clinical setting, the virus may have a significant effect on the treatment of GBM that was observed in MRI. Therefore, we hypothesized that GBM patients inducing alterations in epigenetic features within the tumor after Ad-TD-nsIL-12 treatment might be detected by CSF ctDNA methylation sequencing.

Adenovirus has been used in several studies as a gene transfer vector due to its efficient infectivity [42-44]. Ad-TD-nsIL-12, a new oncolytic adenovirus vaccine, is yet in clinical trials and has not been used on a large scale. Currently, there are no exact criteria for the appropriate dose and time interval of the injection of this virus. However, the virus has good clinical effi-

cacy against GBM, and thus, we attempted to find an appropriate dose and injection interval based on the altered CSF ctDNA methylation level in this patient. We also attempted to find the target that caused the therapeutic response based on the changes in the genome-wide methylation profiles.

Here, we performed ctDNA methylation sequencing on CSF samples collected at different time points from a patient treated with Ad-TD-nsIL-12. The G1-G5 samples were subjected to differential analysis, which showed that most DMR regions were upregulated and a few were downregulated after Ad-TD-nsIL-12 injection. Furthermore, the comparison of logFC of up- and downregulated DMRs revealed that the methylation level of most genes changed after the first injection of Ad-TD-nsIL-12 and returned to the original level after 70 days, while that of some genes would return to the original level after the second injection of Ad-TD-nsIL-12 after 82 days. Therefore, we inferred that the second injection dose of Ad-TD-nsIL-12 (1.8×10^{11} viral particles) may exert a longer effect than the first injection dose. In another study, oncolytic adenovirus DNX-2401 had a prolonged survival outcome for glioma at a dose of 3×10^{10} vp [10]. Combined with the results from GBM ctDNA methylation sequencing, it could be deduced that Ad-TD-nsIL-12 has improved treatment outcomes at a dose of 1.8×10^{11} vp. In addition, patients depicted polycystic degradation on MRI after the second injection of Ad-TD-nsIL-12, which was similar to the MRI of herpes simplex virus type 1 (HSV-1) G207 [45]. This might explain the altered methylation profile. Furthermore, by comparing the repeatedly changed DMRs, DMRs of G3 *vs*. G1 samples, and differential genes of T3 *vs*. T1 tumor tissue samples, we identified 26 genes that co-existed in CSF and tissue samples, and 4 genes co-existed among the three (tissue group, CSF group and changing group after injection); hence, we concluded that these 30 genes might have a diagnostic, prognostic, and efficacy assessment for GBM.

On the other hand, we performed GO and KEGG pathway analysis of the genes corresponding to the DMRs of promoters between the five sets of CSF samples from this patient. The GO analysis displayed that when 1 mL of 3×10^{10} vp/mL of Ad-nsIL-12 was injected per channel, the BPs in the DMRs were related to protein assembly and modification of cell cycle changes and DNA damage. Conversely, when 1.5 mL of 3×10^{10} vp/mL of Ad-TD-nsIL-12 per channel was injected, the BPs in DMRs were involved in the positive regulation of the tumor necrosis factor signaling pathway. These results suggested that Ad-TD-nsIL-12 exerts an anti-tumor effect at an injected dose of 3×10^{10} vp (1.5 mL per channel), which should be combined with this patient's imaging results shorter than 70 days between injections. However, based on subsequent clinical studies, we found that Ad-TD-nsIL-12 had a better therapeutic effect at an injection interval of fewer than 3 weeks, but due to our small sample size and short clinical trials, this conclusion needs to be substantiated by a large number of clinical trials. In addition, four of the top eight pathways, namely apoptosis, alcoholism, neutrophil extracellular trap formation, and systemic lupus erythematosus, with enrichment scores in the KEGG pathway analysis, had overlapping changes. Therefore, we used these four pathways to analyze the enrichment scores of the KEGG pathway. The intersection of these four KEGG pathways revealed that the fold-change in 6 genes, *ACTB*, *RIPK1*, *PARP2*, *H2AFB1*, *H2AFB2*, and *H2AFB3*, was upregulated after viral injection, and then downregulated after 70-82 days. This phenomenon might indicate that the changes in these genes may be due to the injection of Ad-TD-nsIL-12. However, we knocked them out in subsequent studies since 3 genes, *H2AFB1*, *H2AFB2*, and *H2AFB3*, were not expressed in tissue samples. Finally, we included the 30 genes screened in the DMRs in the subsequent study and the 3 genes in the KEGG pathway.

We screened these 33 genes with data from the TCGA database of 698 gliomas and 5 paraneoplastic tissues using univariate analysis, LASSO regression analysis, and multifactorial Cox analysis and finally obtained 8 genes. We speculated that these 8 genes, *ACTB*, *CALN1*, *CCNJL*, *CD5*, *DUSP27*, *GZMB*, *KRT80*, and *LCN2*, may be the hub molecules for response efficacy after Ad-TD-nsIL-12 injection. Hence, we analyzed the differences in the expression of these 8 genes in tumor and paraneoplastic tissues and their effects on patient survival based on clinical data in the TCGA database. The results showed that 4/8 genes (*ACTB*, *CALN1*, *CCNJL*, and *DUSP27*) have significant

differences ($P < 0.05$) between tumor and normal tissues, and all of these 8 genes have a significant effect on patient survival ($P < 0.001$). This phenomenon suggested that the screened 8 genes are critical biomarkers for the diagnosis and prognosis of GBM. Furthermore, the expression profiles of these 8 genes were significantly correlated with immune cells, and the distribution levels of these immune cells in gliomas were significantly correlated with clinical survival. Ad-TD-nsIL-12 is an immunotherapy approach. Therefore, we speculated that the expression of these 8 genes might control the distribution of immune cells and alter the tumor growth microenvironment, which in turn affects the clinical survival of patients. The expression of these hub genes in tumors may be detected through abnormal methylation of CSF ctDNA, which might have occurred before the alteration of the tumor microenvironment. Based on these conjectures, we constructed a hypothetical map of the interactions between immune cells after injection of over Ad-TD-nsIL-12 (Supplementary Figure 9). However, this is an extrapolation that needs to be confirmed with a large amount of clinical data and experiments.

To further validate the importance of hub genes, we constructed a risk score model based on the expression of these 8 genes. This model accurately predicted the survival of patients; those with high-risk scores had shorter survival than those with low-risk scores. Moreover, the risk score increased with the prolonged survival time of patients, which suggested that the risk score model is in line with conventional knowledge. Nevertheless, based on the available data, it is difficult to obtain clinical follow-up data over a long period, and long follow-up and clinical monitoring are required to further investigate and assess the accuracy of this risk score model in terms of clinical prognosis. On the other hand, the diagnostic model constructed based on the 8 hub genes has high accuracy in the diagnosis of glioma, indicating that these genes can accurately assess the prognosis of patients and diagnose the tumor, thereby providing a new biological marker for the diagnosis and prognostic assessment of glioma.

Although Ad-TD-nsIL-12 was constructed in 2017, it has not yet been widely used in the clinic. Currently, no accurate conclusions have been derived on the exact therapeutic dose and treatment duration of Ad-TD-nsIL-12. In this study, we attempted to deduce the appropriate therapeutic dose and treatment period of Ad-TD-nsIL-12 by studying the changes in the CSF ctDNA methylation profile and gene expression profile of tumor tissues combined with MRI features. Although the appropriate dose range of Ad-TD-nsIL-12 was identified in this study, we could not ascertain the exact therapeutic dose because of our small sample size. Therefore, based on the present findings, we need to validate the appropriate therapeutic dose and treatment period of Ad-TD-nsIL-12.

Acknowledgements

This work was supported by the National Key R&D Program (No. 2019YFC1316104), National Science Foundation of China (No. 22077120), the China Postdoctoral Science Foundation (No. 2019M660715), and The Independent Project of Sanbo Brain Hospital (No. 2022-ZZLX01).

Disclosure of conflict of interest

None.

Address correspondence to: Lixin Ma, Department of Neurosurgery, Beijing Chaoyang Hospital, Capital Medical University, Beijing 100020, P. R. China; Department of Neurosurgery, Sanbo Brain Hospital, Capital Medical University, Beijing 100093, P. R. China. E-mail: mlx_182019@163.com

References

[1] Reifenberger G, Wirsching HG, Knobbe-Thomsen CB and Weller M. Advances in the molecular genetics of gliomas - implications for classification and therapy. Nat Rev Clin Oncol 2017; 14: 434-452.

[2] Shergalis A, Bankhead A 3rd, Luesakul U, Muangsin N and Neamati N. Current challenges and opportunities in treating glioblastoma. Pharmacol Rev 2018; 70: 412-445.

[3] Zhao M, van Straten D, Broekman MLD, Preat V and Schiffelers RM. Nanocarrier-based drug combination therapy for glioblastoma. Theranostics 2020; 10: 1355-1372.

[4] Zhao Y, Liu Z, Li L, Wu J, Zhang H, Zhang H, Lei T and Xu B. Oncolytic adenovirus: prospects for cancer immunotherapy. Front Microbiol 2021; 12: 707290.

[5] Cao GD, He XB, Sun Q, Chen S, Wan K, Xu X, Feng X, Li PP, Chen B and Xiong MM. The onco-

lytic virus in cancer diagnosis and treatment. Front Oncol 2020; 10: 1786.
[6] Carpenter AB, Carpenter AM, Aiken R and Hanft S. Oncolytic virus in gliomas: a review of human clinical investigations. Ann Oncol 2021; 32: 968-982.
[7] Fecci PE and Sampson JH. The current state of immunotherapy for gliomas: an eye toward the future. J Neurosurg 2019; 131: 657-666.
[8] Lukas RV, Wainwright DA, Horbinski CM, Iwamoto FM and Sonabend AM. Immunotherapy against gliomas: is the breakthrough near? Drugs 2019; 79: 1839-1848.
[9] Raja J, Ludwig JM, Gettinger SN, Schalper KA and Kim HS. Oncolytic virus immunotherapy: future prospects for oncology. J Immunother Cancer 2018; 6: 140.
[10] Lang FF, Conrad C, Gomez-Manzano C, Yung WKA, Sawaya R, Weinberg JS, Prabhu SS, Rao G, Fuller GN, Aldape KD, Gumin J, Vence LM, Wistuba I, Rodriguez-Canales J, Villalobos PA, Dirven CMF, Tejada S, Valle RD, Alonso MM, Ewald B, Peterkin JJ, Tufaro F and Fueyo J. Phase I study of DNX-2401 (Delta-24-RGD) oncolytic adenovirus: replication and immunotherapeutic effects in recurrent malignant glioma. J Clin Oncol 2018; 36: 1419-1427.
[11] Wang P, Li X, Wang J, Gao D, Li Y, Li H, Chu Y, Zhang Z, Liu H, Jiang G, Cheng Z, Wang S, Dong J, Feng B, Chard LS, Lemoine NR and Wang Y. Re-designing Interleukin-12 to enhance its safety and potential as an anti-tumor immunotherapeutic agent. Nat Commun 2017; 8: 1395.
[12] Nguyen KG, Vrabel MR, Mantooth SM, Hopkins JJ, Wagner ES, Gabaldon TA and Zaharoff DA. Localized interleukin-12 for cancer immunotherapy. Front Immunol 2020; 11: 575597.
[13] Cicchelero L, Denies S, Haers H, Vanderperren K, Stock E, Van Brantegem L, de Rooster H and Sanders NN. Intratumoural interleukin 12 gene therapy stimulates the immune system and decreases angiogenesis in dogs with spontaneous cancer. Vet Comp Oncol 2017; 15: 1187-1205.
[14] Zhang L, Davies JS, Serna C, Yu Z, Restifo NP, Rosenberg SA, Morgan RA and Hinrichs CS. Enhanced efficacy and limited systemic cytokine exposure with membrane-anchored interleukin-12 T-cell therapy in murine tumor models. J Immunother Cancer 2020; 8: e000210.
[15] Lasek W, Zagozdzon R and Jakobisiak M. Interleukin 12: still a promising candidate for tumor immunotherapy? Cancer Immunol Immunother 2014; 63: 419-435.
[16] Marrugo-Ramirez J, Mir M and Samitier J. Blood-based cancer biomarkers in liquid biopsy: a promising non-invasive alternative to tissue biopsy. Int J Mol Sci 2018; 19: 2877.
[17] Cheng F, Su L and Qian C. Circulating tumor DNA: a promising biomarker in the liquid biopsy of cancer. Oncotarget 2016; 7: 48832-48841.
[18] Constancio V, Barros-Silva D, Jeronimo C and Henrique R. Known epigenetic biomarkers for prostate cancer detection and management: exploring the potential of blood-based liquid biopsies. Expert Rev Mol Diagn 2019; 19: 367-375.
[19] Poulet G, Massias J and Taly V. Liquid biopsy: general concepts. Acta Cytol 2019; 63: 449-455.
[20] Bonner ER, Bornhorst M, Packer RJ and Nazarian J. Liquid biopsy for pediatric central nervous system tumors. NPJ Precis Oncol 2018; 2: 29.
[21] Eguchi A, Kostallari E, Feldstein AE and Shah VH. Extracellular vesicles, the liquid biopsy of the future. J Hepatol 2019; 70: 1292-1294.
[22] Mader S and Pantel K. Liquid biopsy: current status and future perspectives. Oncol Res Treat 2017; 40: 404-408.
[23] Panditharatna E, Kilburn LB, Aboian MS, Kambhampati M, Gordish-Dressman H, Magge SN, Gupta N, Myseros JS, Hwang EI, Kline C, Crawford JR, Warren KE, Cha S, Liang WS, Berens ME, Packer RJ, Resnick AC, Prados M, Mueller S and Nazarian J. Clinically relevant and minimally invasive tumor surveillance of pediatric diffuse midline gliomas using patient-derived liquid biopsy. Clin Cancer Res 2018; 24: 5850-5859.
[24] Huang TY, Piunti A, Lulla RR, Qi J, Horbinski CM, Tomita T, James CD, Shilatifard A and Saratsis AM. Detection of Histone H3 mutations in cerebrospinal fluid-derived tumor DNA from children with diffuse midline glioma. Acta Neuropathol Commun 2017; 5: 28.
[25] Valpione S, Gremel G, Mundra P, Middlehurst P, Galvani E, Girotti MR, Lee RJ, Garner G, Dhomen N, Lorigan PC and Marais R. Plasma total cell-free DNA (cfDNA) is a surrogate biomarker for tumour burden and a prognostic biomarker for survival in metastatic melanoma patients. Eur J Cancer 2018; 88: 1-9.
[26] Luo H, Wei W, Ye Z, Zheng J and Xu RH. Liquid biopsy of methylation biomarkers in cell-free DNA. Trends Mol Med 2021; 27: 482-500.
[27] Strauss SB, Meng A, Ebani EJ and Chiang GC. Imaging glioblastoma posttreatment: progression, pseudoprogression, pseudoresponse, radiation necrosis. Neuroimaging Clin N Am 2021; 31: 103-120.
[28] Ritchie ME, Phipson B, Wu D, Hu Y, Law CW, Shi W and Smyth GK. Limma powers differential expression analyses for RNA-sequencing and microarray studies. Nucleic Acids Res 2015; 43: e47.

[29] Zhong QY, Fan EX, Feng GY, Chen QY, Gou XX, Yue GJ and Zhang GH. A gene expression-based study on immune cell subtypes and glioma prognosis. BMC Cancer 2019; 19: 1116.
[30] Chen B, Khodadoust MS, Liu CL, Newman AM and Alizadeh AA. Profiling tumor infiltrating immune cells with CIBERSORT. Methods Mol Biol 2018; 1711: 243-259.
[31] Puchalski RB, Shah N, Miller J, Dalley R, Nomura SR, Yoon JG, Smith KA, Lankerovich M, Bertagnolli D, Bickley K, Boe AF, Brouner K, Butler S, Caldejon S, Chapin M, Datta S, Dee N, Desta T, Dolbeare T, Dotson N, Ebbert A, Feng D, Feng X, Fisher M, Gee G, Goldy J, Gourley L, Gregor BW, Gu G, Hejazinia N, Hohmann J, Hothi P, Howard R, Joines K, Kriedberg A, Kuan L, Lau C, Lee F, Lee H, Lemon T, Long F, Mastan N, Mott E, Murthy C, Ngo K, Olson E, Reding M, Riley Z, Rosen D, Sandman D, Shapovalova N, Slaughterbeck CR, Sodt A, Stockdale G, Szafer A, Wakeman W, Wohnoutka PE, White SJ, Marsh D, Rostomily RC, Ng L, Dang C, Jones A, Keogh B, Gittleman HR, Barnholtz-Sloan JS, Cimino PJ, Uppin MS, Keene CD, Farrokhi FR, Lathia JD, Berens ME, Iavarone A, Bernard A, Lein E, Phillips JW, Rostad SW, Cobbs C, Hawrylycz MJ and Foltz GD. An anatomic transcriptional atlas of human glioblastoma. Science 2018; 360: 660-663.
[32] Tamura R, Ohara K, Sasaki H, Morimoto Y, Kosugi K, Yoshida K and Toda M. Difference in immunosuppressive cells between peritumoral area and tumor core in glioblastoma. World Neurosurg 2018; 120: e601-e610.
[33] Andersen RS, Anand A, Harwood DSL and Kristensen BW. Tumor-associated microglia and macrophages in the glioblastoma microenvironment and their implications for therapy. Cancers (Basel) 2021; 13: 4255.
[34] Wu X, Zhang Y, Hu T, He X, Zou Y, Deng Q, Ke J, Lian L, He X, Zhao D, Cai X, Chen Z, Wu X, Fan JB, Gao F and Lan P. A novel cell-free DNA methylation-based model improves the early detection of colorectal cancer. Mol Oncol 2021; 15: 2702-2714.
[35] Flavahan WA, Gaskell E and Bernstein BE. Epigenetic plasticity and the hallmarks of cancer. Science 2017; 357: eaal2380.
[36] Hata T, Dal Molin M, Hong SM, Tamura K, Suenaga M, Yu J, Sedogawa H, Weiss MJ, Wolfgang CL, Lennon AM, Hruban RH and Goggins MG. Predicting the grade of dysplasia of pancreatic cystic neoplasms using cyst fluid DNA methylation markers. Clin Cancer Res 2017; 23: 3935-3944.
[37] Hulbert A, Jusue-Torres I, Stark A, Chen C, Rodgers K, Lee B, Griffin C, Yang A, Huang P, Wrangle J, Belinsky SA, Wang TH, Yang SC, Baylin SB, Brock MV and Herman JG. Early detection of lung cancer using dna promoter hypermethylation in plasma and sputum. Clin Cancer Res 2017; 23: 1998-2005.
[38] Bettegowda C, Sausen M, Leary RJ, Kinde I, Wang Y, Agrawal N, Bartlett BR, Wang H, Luber B, Alani RM, Antonarakis ES, Azad NS, Bardelli A, Brem H, Cameron JL, Lee CC, Fecher LA, Gallia GL, Gibbs P, Le D, Giuntoli RL, Goggins M, Hogarty MD, Holdhoff M, Hong SM, Jiao Y, Juhl HH, Kim JJ, Siravegna G, Laheru DA, Lauricella C, Lim M, Lipson EJ, Marie SK, Netto GJ, Oliner KS, Olivi A, Olsson L, Riggins GJ, Sartore-Bianchi A, Schmidt K, Shih IM, Oba-Shinjo SM, Siena S, Theodorescu D, Tie J, Harkins TT, Veronese S, Wang TL, Weingart JD, Wolfgang CL, Wood LD, Xing D, Hruban RH, Wu J, Allen PJ, Schmidt CM, Choti MA, Velculescu VE, Kinzler KW, Vogelstein B, Papadopoulos N and Diaz LA Jr. Detection of circulating tumor DNA in early- and late-stage human malignancies. Sci Transl Med 2014; 6: 224ra24.
[39] Wang Y, Springer S, Zhang M, McMahon KW, Kinde I, Dobbyn L, Ptak J, Brem H, Chaichana K, Gallia GL, Gokaslan ZL, Groves ML, Jallo GI, Lim M, Olivi A, Quinones-Hinojosa A, Rigamonti D, Riggins GJ, Sciubba DM, Weingart JD, Wolinsky JP, Ye X, Oba-Shinjo SM, Marie SK, Holdhoff M, Agrawal N, Diaz LA Jr, Papadopoulos N, Kinzler KW, Vogelstein B and Bettegowda C. Detection of tumor-derived DNA in cerebrospinal fluid of patients with primary tumors of the brain and spinal cord. Proc Natl Acad Sci U S A 2015; 112: 9704-9709.
[40] De Mattos-Arruda L, Mayor R, Ng CKY, Weigelt B, Martínez-Ricarte F, Torrejon D, Oliveira M, Arias A, Raventos C, Tang J, Guerini-Rocco E, Martínez-Sáez E, Lois S, Marín O, de la Cruz X, Piscuoglio S, Towers R, Vivancos A, Peg V, Ramon y Cajal S, Carles J, Rodon J, González-Cao M, Tabernero J, Felip E, Sahuquillo J, Berger MF, Cortes J, Reis-Filho JS and Seoane J. Cerebrospinal fluid-derived circulating tumour DNA better represents the genomic alterations of brain tumours than plasma. Nat Commun 2015; 6: 8839.
[41] Li J, Zhao S, Lee M, Yin Y, Li J, Zhou Y, Ballester LY, Esquenazi Y, Dashwood RH, Davies PJA, Parsons DW, Li XN, Huang Y and Sun D. Reliable tumor detection by whole-genome methylation sequencing of cell-free DNA in cerebrospinal fluid of pediatric medulloblastoma. Sci Adv 2020; 6: eabb5427.
[42] Chang J. Adenovirus vectors: excellent tools for vaccine development. Immune Netw 2021; 21: e6.

[43] Afkhami S, Yao Y and Xing Z. Methods and clinical development of adenovirus-vectored vaccines against mucosal pathogens. Mol Ther Methods Clin Dev 2016; 3: 16030.

[44] Bolinger B, Sims S, Swadling L, O'Hara G, de Lara C, Baban D, Saghal N, Lee LN, Marchi E, Davis M, Newell E, Capone S, Folgori A, Barnes E and Klenerman P. Adenoviral vector vaccination induces a conserved program of CD8+ T cell memory differentiation in mouse and man. Cell Rep 2015; 13: 1578-1588.

[45] Friedman GK, Johnston JM, Bag AK, Bernstock JD, Li R, Aban I, Kachurak K, Nan L, Kang KD, Totsch S, Schlappi C, Martin AM, Pastakia D, McNall-Knapp R, Farouk Sait S, Khakoo Y, Karajannis MA, Woodling K, Palmer JD, Osorio DS, Leonard J, Abdelbaki MS, Madan-Swain A, Atkinson TP, Whitley RJ, Fiveash JB, Markert JM and Gillespie GY. Oncolytic HSV-1 G207 immunovirotherapy for pediatric high-grade gliomas. N Engl J Med 2021; 384: 1613-1622.

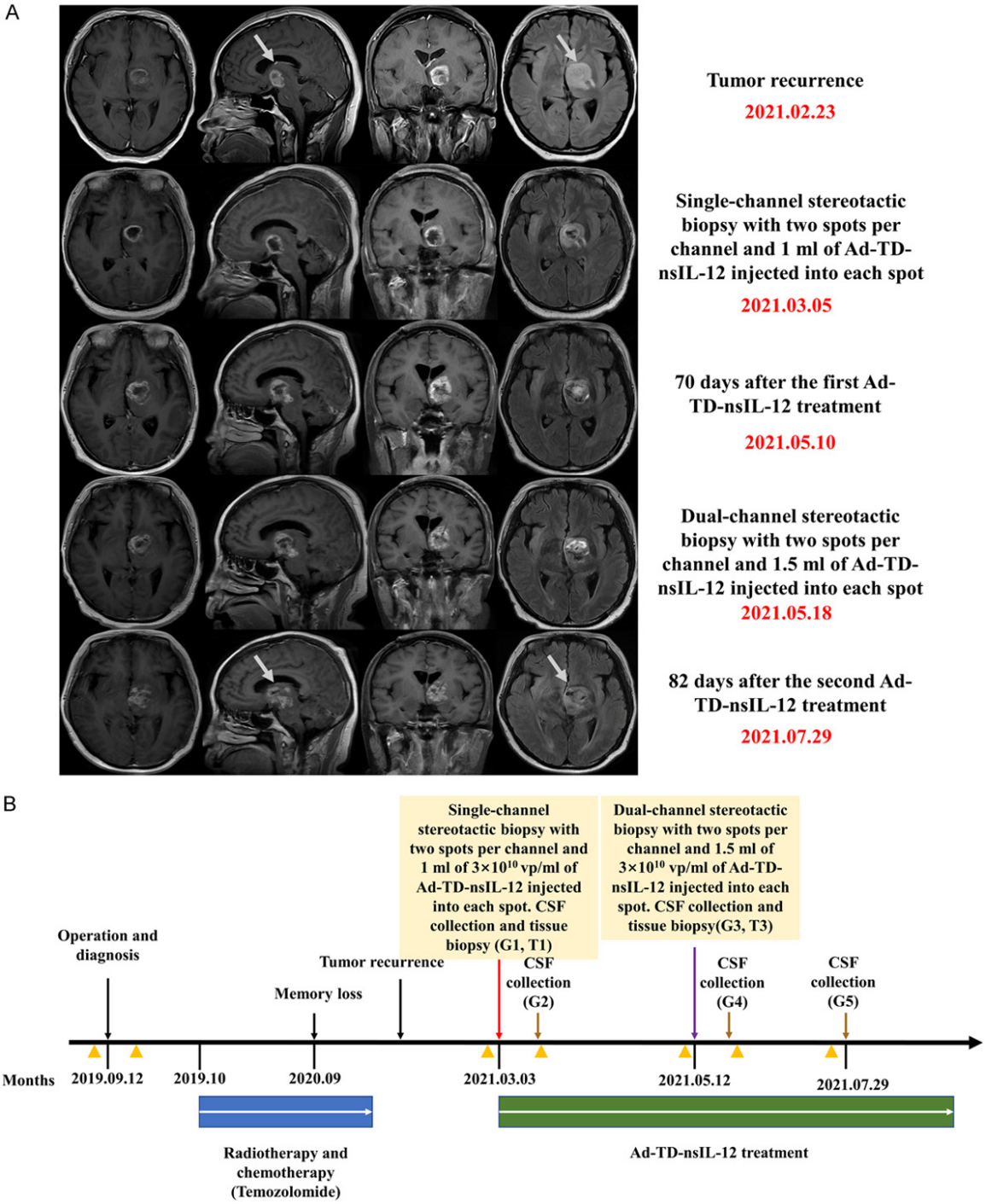

Supplementary Figure 1. MRI and treatment timeline of this GBM patient. A. MRI of patients with GBM treated with Ad-TD-nsIL-12 at different times. The red font indicates the time of the MRI. B. Timeline of this patient's diagnosis, tumor recurrence, and treatment. The yellow triangle indicates the time when the MRI was taken, the red arrow indicates the time of the first injection of Ad-TD-nsIL-12, and the purple arrow indicates the time of the second injection of Ad-TD-nsIL-12, and the brown arrow indicates the time of CSF collection for three of the samples.

Supplementary Table 1. Clinical characteristics of patients

Date	Sample name	Methods of treatment	Tissue collection	CSF collection
2019.9		Radiotherapy and temozolomide	No	No
2021.2	G1/T1	Ad-TD-nsIL-12	Yes	Yes
2021.3	G2	None	No	Yes
2021.5	G3/T3	Ad-TD-nsIL-12	Yes	Yes
2021.6	G4	None	No	Yes
2021.7	G5	None	No	Yes
2021.9	N	None	Yes	No

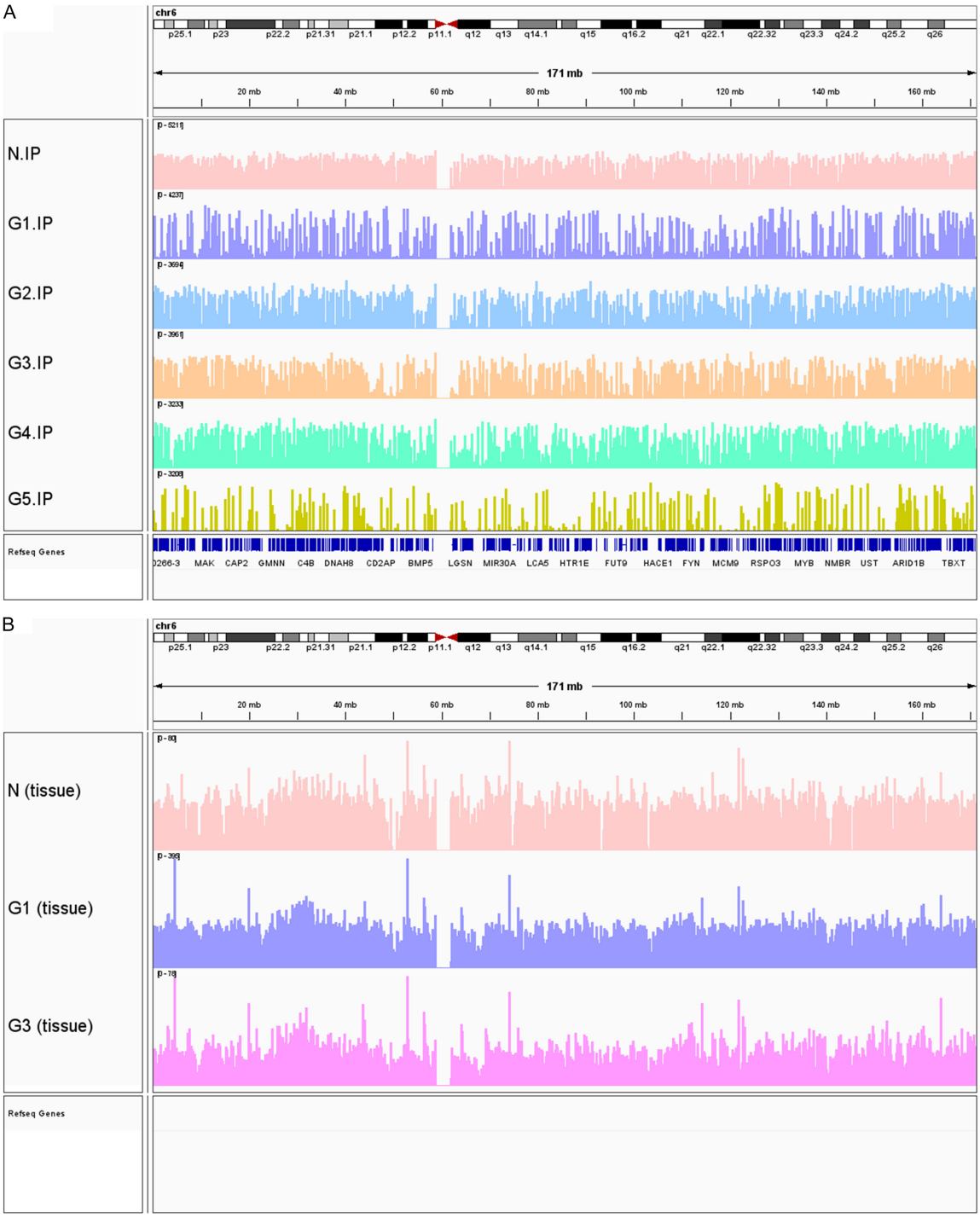

Supplementary Figure 2. Visualization of sample methylation and gene expression using IGV software. A. Methylation levels of CSF ctDNA in five groups of tumor samples and one group of normal samples. The higher the methylation level the more significant the peak. B. Gene expression levels of two tumor tissue samples and one normal tissue sample. The higher the gene expression level, the more significant the peak.

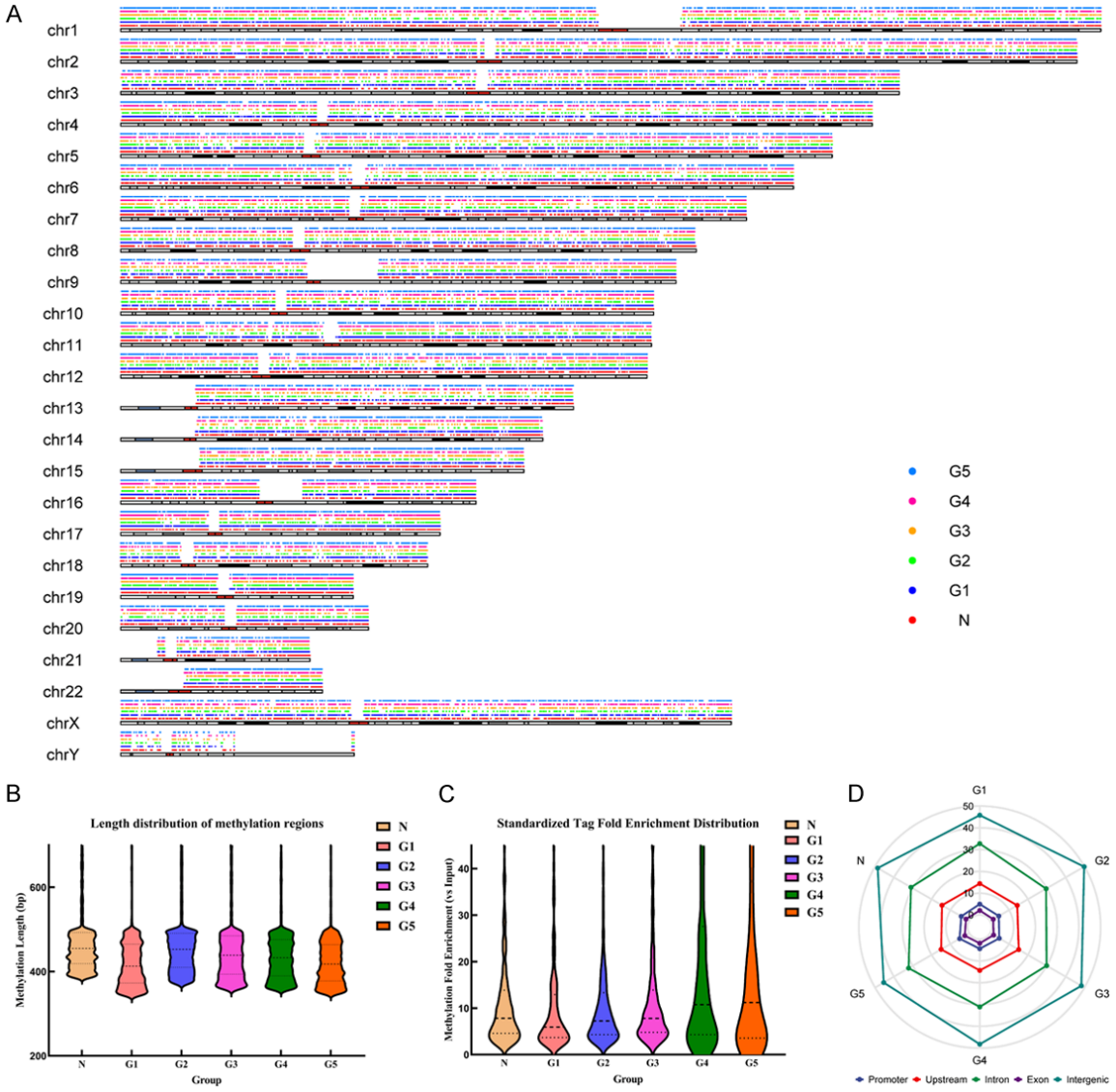

Supplementary Figure 3. Characterization of CSF ctDNA methylation profiles. A. Distribution of methylation regions on chromosomes in each group of samples. B. The length distribution of the methylation region. C. The distribution of methylation fold enrichment for each group of samples compared to the Input sample. D. Percentage distribution of the number of methylated regions on genomic progenitors.

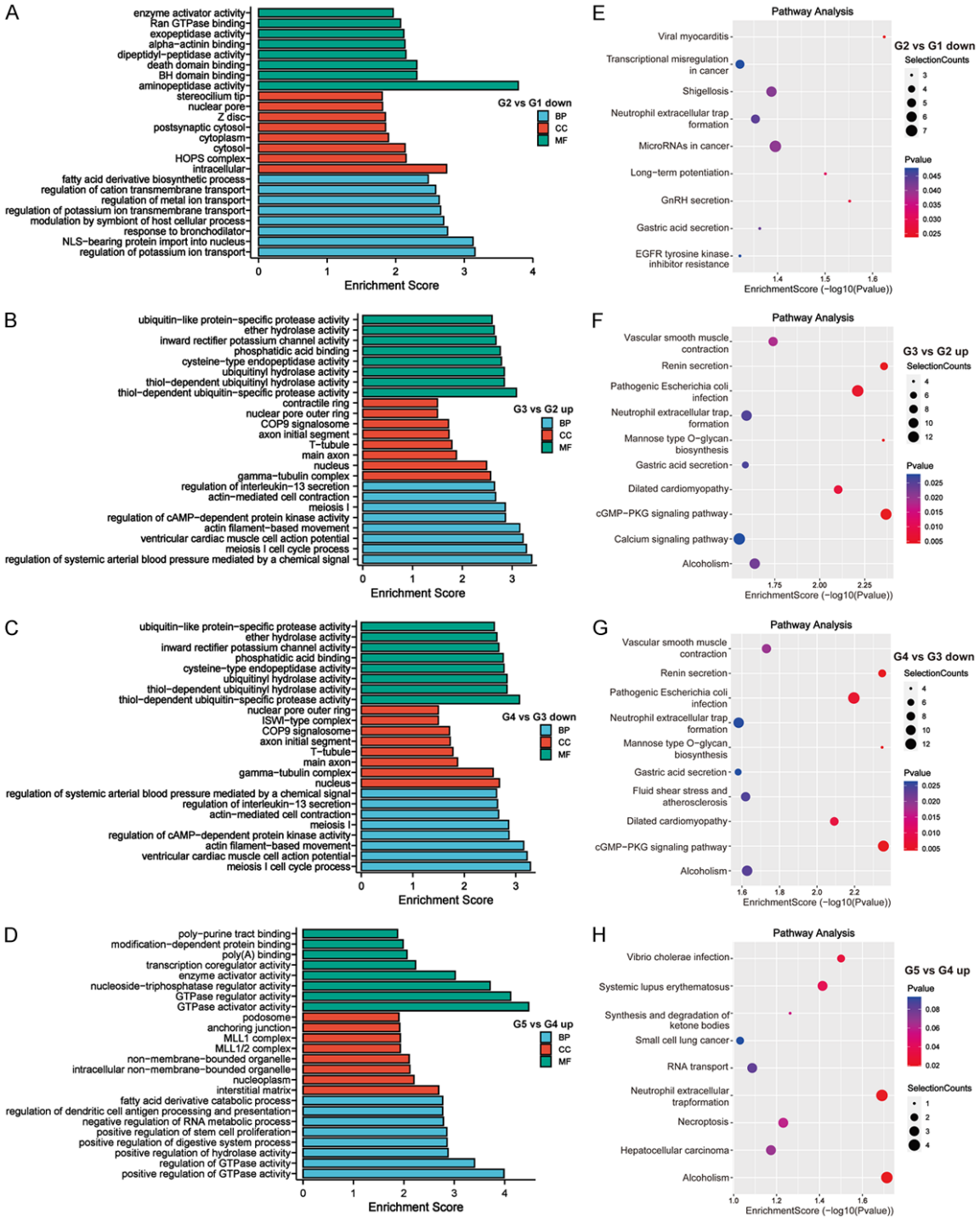

Supplementary Figure 4. GO and KEGG analysis of genes associated with promoter DMRs of CSF ctDNA. A-D. CSF ctDNA promoter DMRs associated with gene enrichment scores for the top 8 terms of GO analysis. E-H. CSF ctDNA promoter DMRs associated gene enrichment fraction of the top 8 of the KEGG pathway.

Supplementary Table 2. The 33 genes were screened for 24 P < 0.05 after univariate COX analysis

id	HR	HR.95L	HR.95H	*p* value
ACTB	1.001289	1.001113	1.001465	9.46E-47
RIPK1	1.305065	1.257542	1.354384	5.94E-45
CCNJL	2.154157	1.882366	2.465191	7.00E-29
GZMB	1.546155	1.424568	1.678121	1.85E-25
PLAU	1.019152	1.015517	1.0228	2.32E-25
CD2	1.264262	1.20852	1.322575	2.15E-24
CCR2	1.958554	1.707111	2.247033	8.94E-22
KRT80	3.067507	2.438723	3.858413	1.00E-21
CD5	2.325016	1.934853	2.793855	2.21E-19
CALN1	0.794533	0.755201	0.835913	6.75E-19
LY86	1.023058	1.016321	1.029839	1.36E-11
PARP2	0.852007	0.810361	0.895793	3.76E-10
KLF5	1.324002	1.201483	1.459014	1.47E-08
IER3	1.021528	1.012716	1.030417	1.45E-06
ELF3	1.963618	1.483734	2.598712	2.36E-06
DUSP27	0.341935	0.209762	0.55739	1.67E-05
C1QL3	0.941448	0.901157	0.983541	0.006859
MUC5B	3.77E-08	3.08E-14	0.046107	0.016839
LCN2	1.070907	1.01092	1.134454	0.019846
NGF	1.124997	1.018267	1.242914	0.020563
EBI3	1.03086	1.001897	1.06066	0.036587
CRTAM	1.160825	1.007474	1.337519	0.039116
SCML4	1.529828	1.015027	2.305728	0.042233
MUC4	0.164313	0.027955	0.965808	0.045667

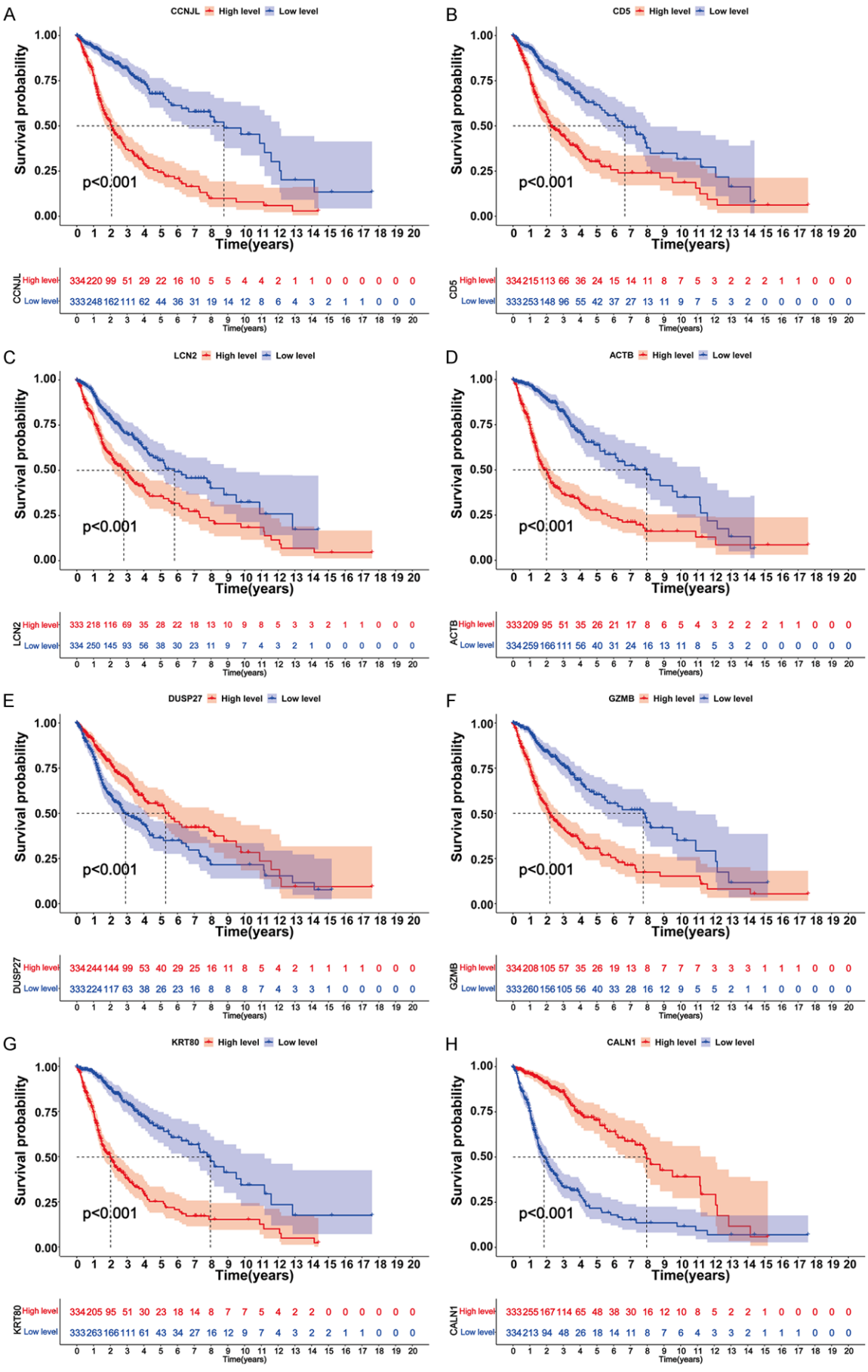
A
CCNJL High level Low level
Survival probability
p<0.001
Time(years)
CCNJL High level 334 220 99 51 29 22 16 10 5 5 4 4 2 1 1 0 0 0 0 0 0
Low level 333 248 162 111 62 44 36 31 19 14 12 8 6 4 3 2 1 1 0 0 0
B
CD5 High level Low level
Survival probability
p<0.001
Time(years)
CD5 High level 334 215 113 66 36 24 15 14 11 8 7 5 3 2 2 2 1 1 0 0 0
Low level 333 253 148 96 55 42 37 27 13 11 9 7 5 3 2 0 0 0 0 0 0
C
LCN2 High level Low level
Survival probability
p<0.001
Time(years)
LCN2 High level 333 218 116 69 35 28 22 18 13 10 9 8 5 3 3 2 1 1 0 0 0
Low level 334 250 145 93 56 38 30 23 11 9 7 4 3 2 1 0 0 0 0 0 0
D
ACTB High level Low level
Survival probability
p<0.001
Time(years)
ACTB High level 333 209 95 51 35 26 21 17 8 6 5 4 3 2 2 2 1 1 0 0 0
Low level 334 259 166 111 56 40 31 24 16 13 11 8 5 3 2 0 0 0 0 0 0
E
DUSP27 High level Low level
Survival probability
p<0.001
Time(years)
DUSP27 High level 334 244 144 99 53 40 29 25 16 11 8 5 4 2 1 1 1 1 0 0 0
Low level 333 224 117 63 38 26 23 16 8 8 8 7 4 3 3 1 0 0 0 0 0
F
GZMB High level Low level
Survival probability
p<0.001
Time(years)
GZMB High level 334 208 105 57 35 26 19 13 8 7 7 7 3 3 3 1 1 1 0 0 0
Low level 333 260 156 105 56 40 33 28 16 12 9 5 5 2 1 1 0 0 0 0 0
G
KRT80 High level Low level
Survival probability
p<0.001
Time(years)
KRT80 High level 334 205 95 51 30 23 18 14 8 7 7 5 4 2 2 0 0 0 0 0 0
Low level 333 263 166 111 61 43 34 27 16 12 9 7 4 3 2 2 1 1 0 0 0
H
CALN1 High level Low level
Survival probability
p<0.001
Time(years)
CALN1 High level 333 255 167 114 65 48 38 30 16 12 10 8 5 2 2 1 0 0 0 0 0
Low level 334 213 94 48 26 18 14 11 8 7 6 4 3 3 2 1 1 1 0 0 0

Supplementary Figure 5. A-H. The samples were divided into high- and low-expression groups according to the expression differences in 8 genes, and KM survival curves were plotted according to their OS. Red indicates a high expression level, and blue indicates a low-expression level.

Supplementary Table 3. 22 immune cells about OS

Immune cells	Associated with increased OS	No association with OS	Associated with decreased OS
B cells naive		√	
B cells memory		√	
Plasma cells		√	
T cells CD8	√		
T cells CD4 naive			√
T cells CD4 memory resting		√	
T cells CD4 memory activated	√		
T cells follicular helper		√	
T cells regulatory (Tregs)	√		
T cells gamma delta	√		
NK cells resting		√	
NK cells activated			√
Monocytes			√
Macrophages M0	√		
Macrophages M1	√		
Macrophages M2	√		
Dendritic cells resting		√	
Dendritic cells activated		√	
Mast cells resting	√		
Mast cells activated			√
Eosinophils			√
Neutrophils	√		

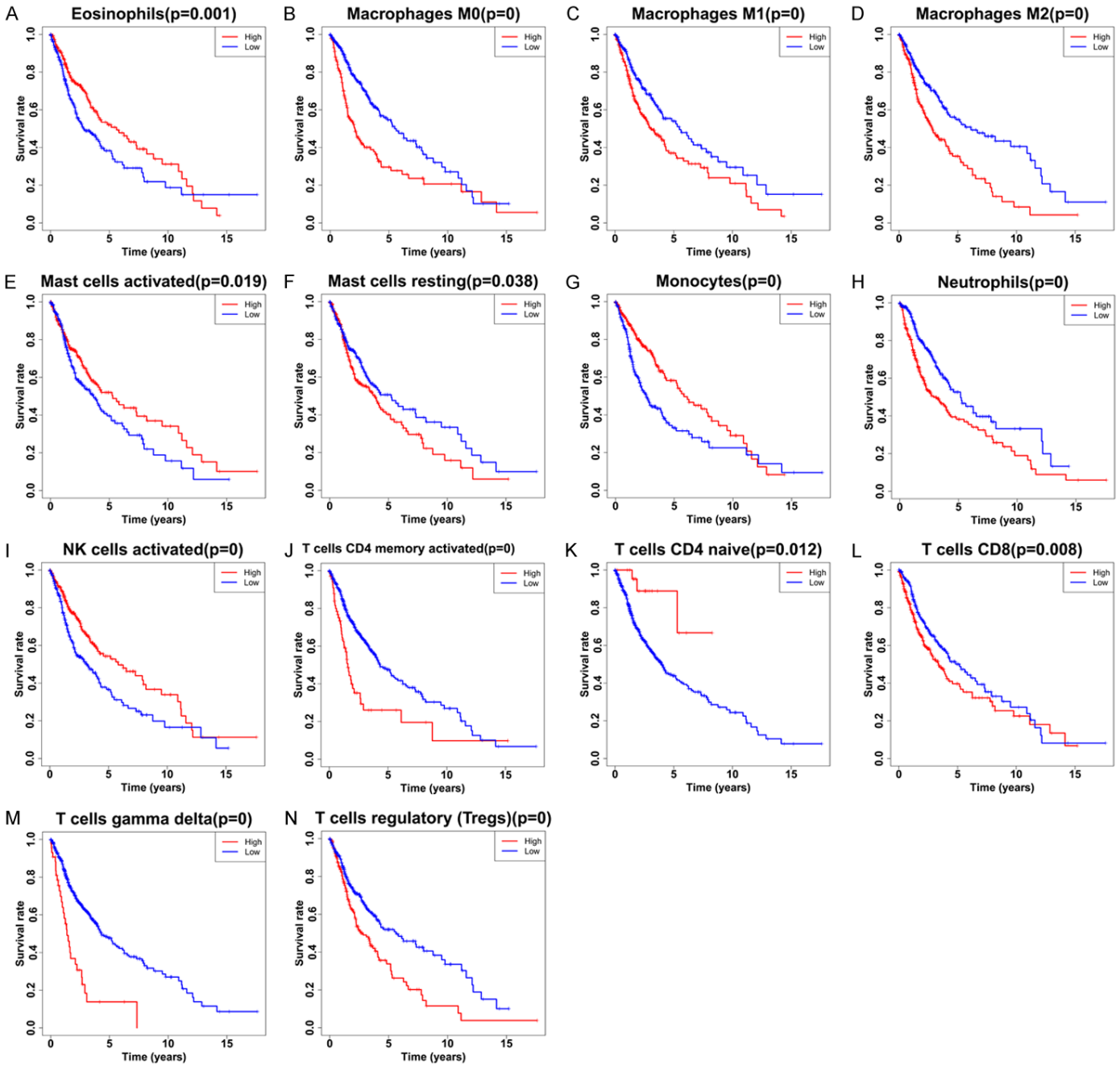
A
Eosinophils(p=0.001)
B
Macrophages M0(p=0)
C
Macrophages M1(p=0)
D
Macrophages M2(p=0)
E
Mast cells activated(p=0.019)
F
Mast cells resting(p=0.038)
G
Monocytes(p=0)
H
Neutrophils(p=0)
I
NK cells activated(p=0)
J
T cells CD4 memory activated(p=0)
K
T cells CD4 naive(p=0.012)
L
T cells CD8(p=0.008)
M
T cells gamma delta(p=0)
N
T cells regulatory (Tregs)(p=0)
High
Low
Survival rate
Time (years)

Supplementary Figure 6. A-N. KM survival curves of immune cells, red indicates a high degree of infiltration and blue indicates a low degree of infiltration ($P < 0.05$).

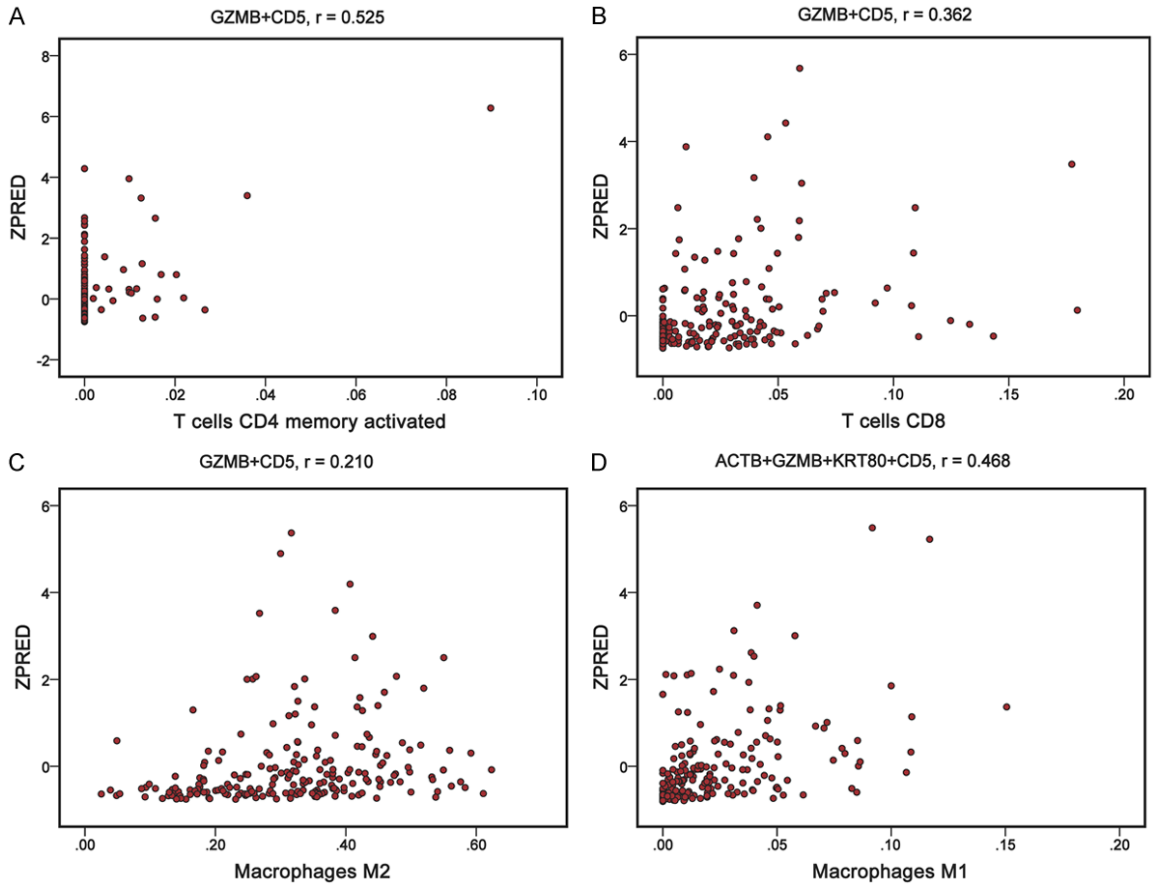

Supplementary Figure 7. Multi-correlation analysis of hub genes significantly associated with immune cells. A-D. Multi-correlation analysis between hub genes and T cells CD4 memory activated, T cells CD8, macrophage M0, and macrophage M1.

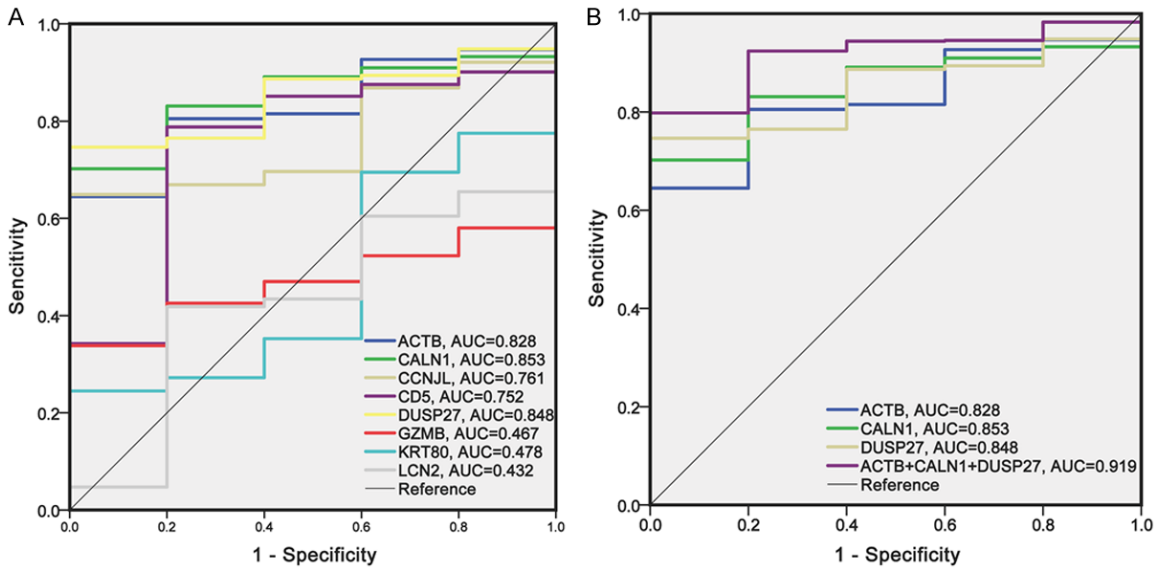

Supplementary Figure 8. Diagnostic model construction using 8 hub genes. A, B. The combined diagnostic ROC for hub genes.

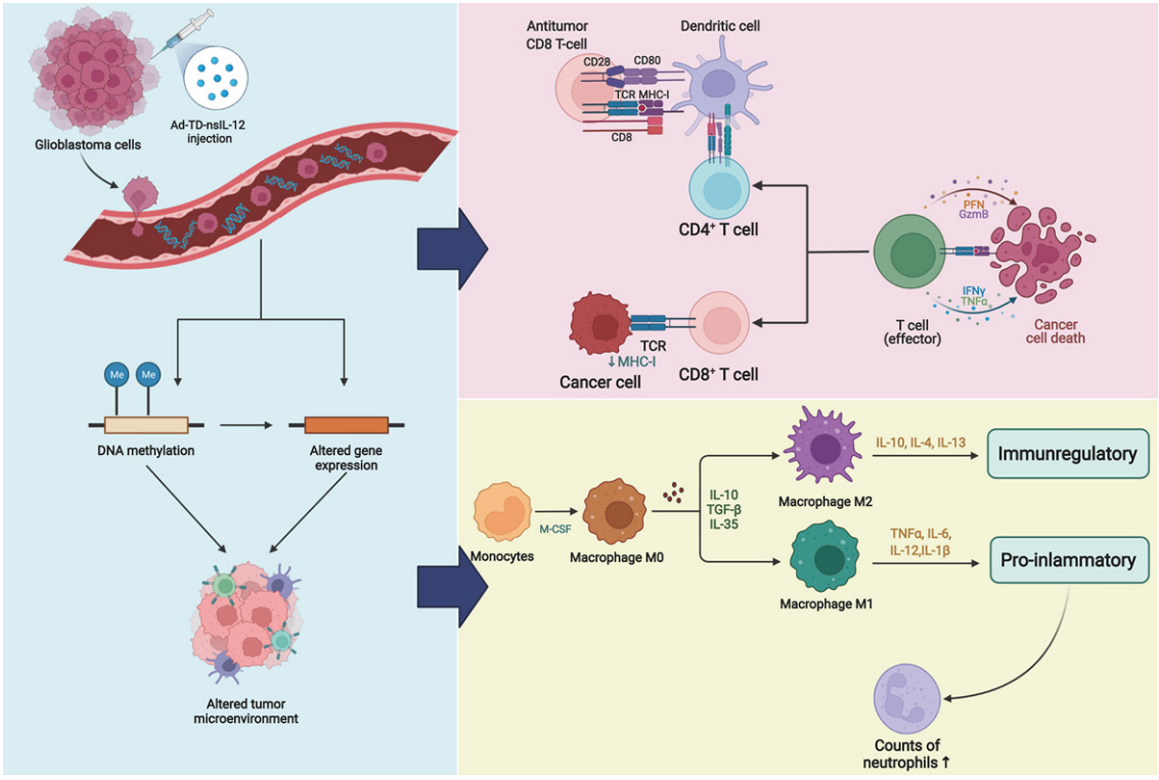

Supplementary Figure 9. Hypothetical graph of the role of inter-immune cell relationships induced by the injection of over Ad-TD-nsIL-12 (Created with BioRender.com).